JOURNAL OF GEOPHYSICAL RESEARCH, VOL. 86, NO. C5, PAGES 4103–4124, MAY 20, 1981

Energy Transfer Among Internal Gravity Modes: Weak and Strong Interactions

I. ORLANSKI

Geophysical Fluid Dynamics Laboratory/NOAA, Princeton University, Princeton, New Jersey 08540

C. P. CERASOLI

Geophysical Fluid Dynamics Program, Princeton University, Princeton, New Jersey 08540

The general characteristics of the energy spectrum for internal gravity waves in the ocean are well known from the large body of recent experimental observations. The theoretical understanding has not developed at the same rate, perhaps due to the limitation of linear or quasi-linear theories, which can cope only with weak interaction processes and are inadequate for representing the more violent and sporadic wave breaking processes present in nature. A detailed study of energy transfer among two-dimensional internal gravity modes in a fully nonlinear regime was performed. Wave-wave interactions and overturning were included in the solutions of a two-dimensional numerical model, and the results are presented here. A background spectrum of finite amplitude, random internal gravity wave field was generated by a long time integration of a two-dimensional model with random body forcing. Over this background field, two sets of experiments were performed: spike-random, where energy at low, medium, and high wave numbers were introduced and integrated in time, and band-random, where energy was introduced over a band of wave numbers instead of introducing only discrete modes. The results can be summarized as follows. Multiple triad interactions will result in a filling of the energy spectrum when energy is introduced in a particular band of wave numbers. For bands where the energy level is high enough to result in nonlinear time scales of only a few intrinsic periods, wave-wave interactions (resonant and nonresonant) provide the mechanism for filling the spectrum. The energy transfer becomes more and more rapid with increasing energy, and no universal spectrum appears to result from these processes. As the energy input increases, energy will accumulate in high wave numbers until localized instabilities (overturning) occur. From that point on, these high wave numbers will remain at a saturation such that any additional energy input at the saturated band, either directly or via wave-wave interactions, will result in localized mixing. On the other hand, additional energy input at bands other than the saturated band will result in an increase of low and medium wave band energy (via wave-wave interactions) until an equilibrium level is achieved. The equilibrium level of any particular band will depend on the high wave number bands' being saturated. For instance, any energy above the equilibrium at low wave numbers will produce localized mixing in physical space almost instantaneously. This does not mean that the low wave numbers are saturated, as their energy levels can be much lower than a saturation level. What takes place at or near an equilibrium level is that the contributions from high and low wave numbers result in localized regions in physical space where the criterion for instability is almost met. In fact, this superposition effect means that low and medium wave numbers are far from meeting any breaking criterion when taken individually, yet cannot tolerate any additional input energy when in the presence of a saturated band of high wave numbers. It was found also that the dissipation is approximately constant over the wave numbers and small compared with the large transfer of energy between neighboring waves. However, if bands of waves are considered, very little energy is transferred between neighboring bands above the equilibrium level. Rather, a direct cascade of energy from low to high wave numbers occurs due to localized instabilities which result in overturning, and it is this amount of energy flux which is dissipated by the high wave numbers.

1. INTRODUCTION

The important role of internal gravity waves in geophysical systems has been recognized for some time, especially in the case of very stable systems such as the ocean. The large body of evidence for the existence of oceanic internal gravity waves began with the temperature measurements of *LaFond* [1949] and *Charnock* [1965] and the long time current meter records obtained by *Webster* [1969] and *Fofonoff and Webster* [1971]. The number and quality of internal gravity wave field measurements have grown dramatically since the early 1970's, and a variety of techniques has been employed to obtain measurements suitable to give wave number and frequency spectra in different parts of the world oceans. Concurrent with the observational advances, our theoretical knowledge of internal gravity waves has grown considerably. A lucid exposition of oceanic internal waves can be found in *Thorpe*'s [1975] review article, and an up-to-date interpretation of the latest advances can be found in *Phillips* [1977].

The purpose of this study is to investigate the means by which energy is transferred among internal gravity waves. The transfer of energy in weakly interacting flows is characterized by resonant interactions in which the interaction time scale is much greater than the component wave periods [*Müller and Olbers,* 1975; *McComas and Bretherton,* 1977]. The energy transfers occurring in a more nonlinear system, where interaction time scales can be larger or of the same order as the wave period (strong interaction), were practically untreated. In the present study, we will discuss the dynamics of waves and the building of an energy spectrum in such a nonlinear regime. Such a regime is perhaps more characteristic of the natural state of the ocean with regard to internal gravity waves. Let us therefore summarize the highlights of the scien-

Paper number 80C1388.

tific works which have provided today's picture of internal waves in the ocean.

Characteristics of the energy density as a function of horizontal wave number have emerged from data based on towed sensor [*Charnock,* 1965; *Katz,* 1975] and moored spatial array measurements (internal wave experiment (IWEX), *Müller et al.* [1978]). Basically, one has that the energy spectrum is horizontally isotropic and depends upon horizontal wave number as the −2.5 power. Measurements of vertical structure [*Hayes,* 1975; *Leaman and Sanford,* 1975; *Müller et al.,* 1978] show that a model representation is appropriate for high-frequency internal waves (close to the local buoyancy frequency), while low-frequency waves (close to the local inertial frequency) may be represented as a superposition of freely propagating upward and downward waves, where the vertical energy fluxes need not be balanced. Long, fixed point records of horizontal velocities were obtained by *Fofonoff and Webster* [1971] and *Gould et al.* [1974], while *Cairns* [1975] obtained long isotherm displacement records using an instrumented buoy which 'yo-yoed' about a fixed isotherm. The spectral picture is one where energy is predominantly contained in a band between the local inertial frequency and the local buoyancy frequency. The energy density may be approximated by an ω^{-2} (ω is the frequency) dependence with predominant spectral peaks at the local inertial and tidal frequencies. A less pronounced peak exists near the local buoyancy frequency, and a sharp roll-off in energy occurs beyond this frequency. Finally, the similarity of the appropriately normalized energy spectra from various world ocean sites can be interpreted as the existence of a degree of universality for the spectral band representing oceanic internal gravity waves.

An empirical formulation relating wave number and frequency spectra for internal waves was proposed by *Garrett and Munk* [1972*a*, 1975] and provided a consistent framework for the large body of data taken with various techniques. Universality and horizontal isotropy, as well as the kinematic characteristics of internal gravity waves, were invoked to formulate their empirical relations. It is clearly understood that this formulation does not contain any description of the dynamics which give rise to the observed spectra. The recurring spectral shape obtained from field data, universal or not, opens the question of what are the mechanisms which achieve this spectral shape and what is the time scale for relaxing to this shape, since the oceans are continually being forced in various spectral bands. The problem of energy distribution among internal waves and the description of the energy spectrum in terms of such transfers have been studied since the last decade.

Theoretical work on the slow or weak interaction for three discrete, resonantly interacting waves was done by *Bretherton* [1964] and *Phillips* [1966], while *Davis and Acrivos* [1967] were the first to experimentally observe triad resonance, using a two-layer stratified fluid. The time scale for such interactions was found to be inversely proportional to the square root of the total triad energy. Typically, this time scale is much greater than the wave periods, justifying the weak interaction assumption. Laboratory experiments on triad resonance in linearly stratified fluids were performed for horizontally propagating internal waves by *Martin et al.* [1972] and for modes by *McEwan et al.* [1972]. These experiments showed that whenever a single triad is initiated, other resonant triads will also be excited, and that the wave-wave interaction is stronger for higher frequency waves than for the lower-frequency waves. This cascade phenomenon implies that three discrete, interacting waves is not a good model of wave-wave interaction, even in the weak regime, since the simultaneous excitation of other triads is continually occurring. It is apparent from the observed oceanic spectra that wave-wave interactions must be treated in a continuous spectrum, and theoretical work along these lines was done by *Müller and Olbers* [1975] and *McComas and Bretherton* [1977] using a methodology developed by *Hasselmann* [1966, 1967]. McComas and Bretherton studied the manner in which weakly interacting waves decay in different parts of the spectrum, and interaction coefficients were calculated only for resonantly interacting waves. However, their results show that the interaction time could be very rapid (a few periods). This opens the question of whether only resonantly interacting waves should be considered, or perhaps, waves which are nonresonantly forced must also be considered. More important is the question of wave breaking versus wave-wave interactions as a mechanism for limiting wave amplitudes. *Phillips* [1977] discusses a scenario whereby the lower modes are limited by wave breaking rather than the transfer of energy to higher modes. Two types of wave breaking can occur: (1) a shear instability, as discussed by *Phillips* [1966], which requires a local Richardson number to be less than ¼, and (2) a finite amplitude gravitational instability discussed by *Orlanski and Bryan* [1969] and *Orlanski* [1972] which requires that a locally unstable stratification exists. (The criterion for a single wave is that the fluid parcel velocity exceeds the phase velocity.) Both types can occur in the ocean, and their occurrence is probably enhanced due to the presence of a large number of waves. That is, a single wave may not satisfy either breaking condition, but when the many other waves are superimposed, the breaking conditions may be satisfied.

The concern over which breaking mechanism is operating in the ocean may be important for the estimation of dissipation due to wave breaking, and for predicting a critical wave spectrum amplitude. However, previous attempts to enhance the importance of shear instability or gravitational instability [*Garrett and Munk,* 1972*b*; *Frankignoul,* 1972] show contradictory results. In fact, *Eriksen* [1978] recently has found that both types of breaking are possible and breaking appears equally likely at all frequencies in the internal wave range. Perhaps, the simple picture put forward by *Phillips* [1966] should be reconsidered. The scenario is one where the amplitude of the low modes is limited by localized shear instability, while the amplitude of the higher modes is determined by wave-wave interactions. Two features of the oceanic spectra work against such a model. First, wave breaking appears to be occurring at all frequencies (modes) and, second, the interaction times associated with the Garrett and Munk spectrum are the same order of magnitude as typical wave periods [*McComas and Bretherton,* 1977]. This 'rapid' interaction time is inconsistent with the weak interaction approximations.

Orlanski and Cerasoli [1979] treated the wave-wave interaction problem for nonrotating two-dimensional internal gravity waves using (1) the integration of the gyroscopic equations, (2) a numerical simulation which allowed the modeling of dissipation due to wave breaking, and (3) laboratory experiments. The study provided the logical framework for treating wave systems with an increasing number of degrees of freedom, and the laboratory data provided verification of the numerical simulation. The sensitivity of three and four wave triad interactions to the presence of other waves was clearly

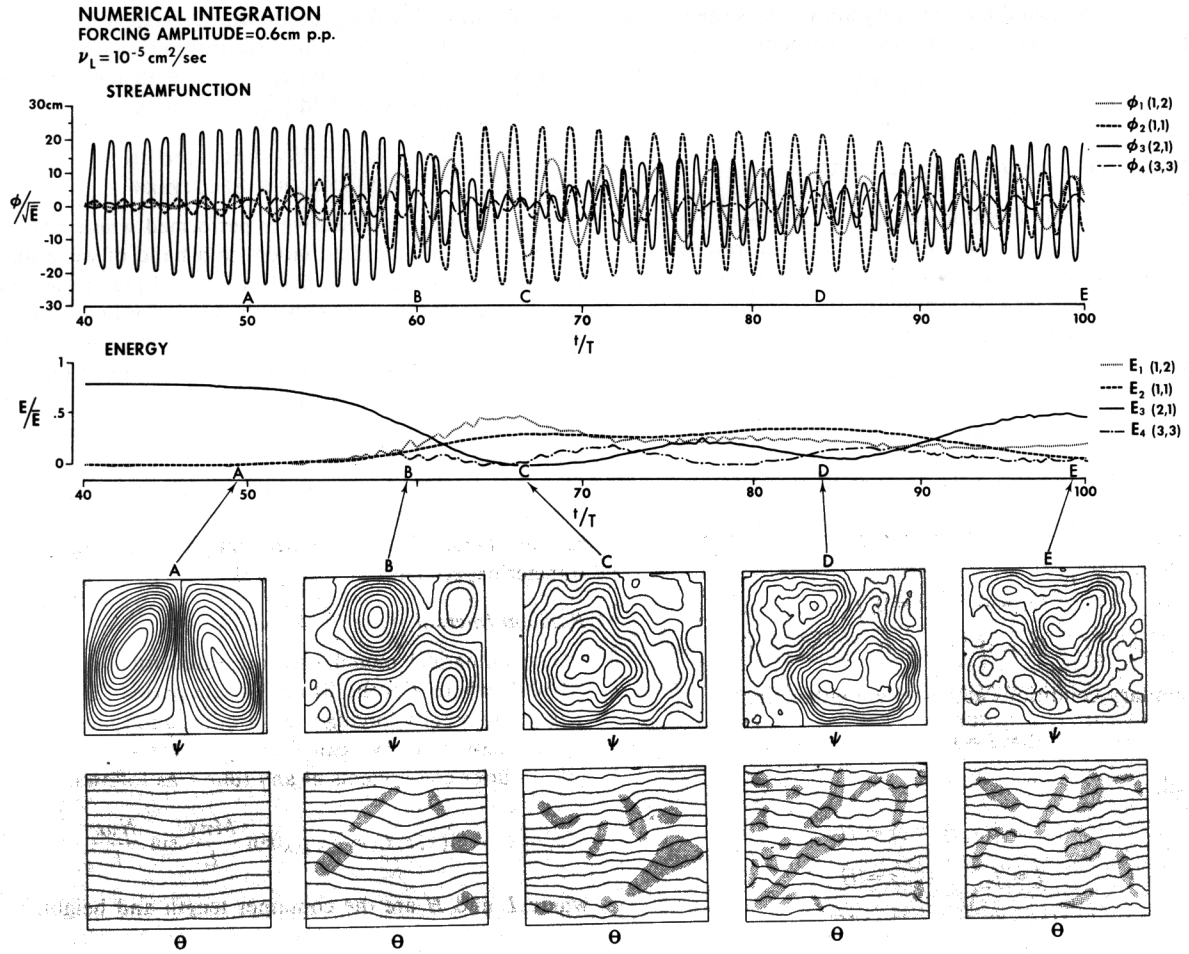

Fig. 1. Stream function and energy versus time from the integration shown in Figure 1 are presented in the upper portion. Stream function and density perturbation contours at various times are shown in the lower portion, and the stippling in the plot shows regions of probable wave breaking.

demonstrated, and the importance of wave breaking for limiting wave amplitudes was established. A number of results from that study can be summarized using Figure 1. The numerical simulation was used to model the growth due to surface forcing of a mode unstable to triad resonance. By a time of 40 buoyancy periods (T), the forced wave has been established, as seen in the streamline contours in the lower portion of the figure. The field was Fourier decomposed and the stream function and energy of the four resonantly interacting modes are shown in the upper and middle portion of Figure 1, respectively. The triad partners grow at the expense of the forced mode from approximately $40T$ to $60T$, and the evolution is similar to that predicted by classical theory of triad interaction. After this point, the flow field becomes complex as the four primary triad waves attain comparable amplitudes and other nonprimary waves are excited. Wave breaking is a prominent feature, and areas of overturning are marked with stippling in the isopycnic contours. Results indicated that the saturation amplitude of the forced mode was controlled by wave breaking rather than by triad interactions.

The present work continues this treatment of nonrotating, two-dimensional internal waves where the dissipative effect of wave breaking can be realistically modeled. In particular, the manner in which wave breaking and wave-wave interactions act to maintain the amplitude and shape of internal wave spectra is studied. The large number of waves necessary to accurately model a spectrum of interacting, finite amplitude internal waves necessitated using a two-dimensional model to keep the problem tractable. One purpose of this work was to demonstrate the importance of wave breaking in determining spectral amplitudes, and having established this, one may assume the wave breaking will be as important (if not more so) in three dimensions where a rapid cascade of energy to small scales occurs. In section 2, the equations of motion are presented along with a description of the numerical model. The creation of a spectrum of random, internal gravity waves is discussed in section 3, and the characteristics of this internal wave field are presented. This background field of waves was perturbed by introducing energy either in discrete modes, or in a band of wave numbers, and the results are discussed in sections 4 and 5, respectively. The energy fluxes and dissipation are presented in section 6. Sensitivity studies on the equilibrium spectrum described in section 5 are shown in section 7. Section 8 includes the summary and conclusions.

2. Equations of Motion: Truncated Spectra and Two-Dimensional Numerical Model

Let us consider a two-dimensional container of length L and height H filled with a linearly stratified fluid of density ρ

$= \rho_0(1 + \beta z)$. The two dimensionality allows the system to be described by the following equations for vorticity and density:

$$\xi_t - J(\psi, \xi) = g\Theta_x + \nabla(\nu\nabla\xi) \quad (1)$$

$$\xi = \nabla^2\psi \quad (2)$$

$$\Theta_t - J(\psi, \Theta) = \beta\psi_x + \nabla(\kappa\nabla\Theta) \quad (3)$$

where ψ is the stream function and $u = \psi_z$, $w = -\psi_x$. Horizontal and vertical velocity components are u and w, respectively, and Θ is the density departure divided by ρ_0, $\Theta = (\rho - \bar{\rho})/\rho_0$. The eddy conductivity and diffusivity are κ and ν, and their proper form will be discussed in section 3.

Free slip boundary conditions are used for stream function and vorticity at the side walls and bottom boundary,

$$\psi = \xi = 0 \qquad x = 0, L$$

$$\psi = \xi = 0 \qquad z = 0$$

and the adiabatic conditions for the density perturbation are used,

$$\Theta_x = 0 \qquad x = 0, L$$

$$\Theta_z = 0 \qquad z = 0$$

The boundary conditions at $z = H$ are either rigid,

$$\psi = \xi = 0 \qquad z = H$$

or forced,

$$\psi = f(x, t) \qquad z = H$$

$$\xi = f_{zz} \qquad z = H$$

$$\Theta_z = 0 \qquad z = H$$

where $f(x, t)$ is prescribed.

The vorticity and density equations (1) and (3) were integrated with a finite difference scheme. A rectangular tank was modeled with 51 horizontal points and 61 vertical points, and allowed the resolution of some 200 waves. The details of the model were described by *Orlanski and Ross* [1973]; the model uses a standard leap frog, energy-conserving scheme with an exact Poisson solver for the stream function. The height and length of the tank were 81 and 150 cm, respectively, for comparative purposes with laboratory experiments.

The effects due to subgrid scale motion were modeled with a method detailed elsewhere [*Orlanski and Ross,* 1973; *Orlanski et al.,* 1974] by use of an eddy diffusivity and conductivity defined as follows:

$$\nu = \frac{\nu_L}{\kappa_L}\left[1 + \frac{\nu_{NL/\nu_L}}{\kappa_{NL/\kappa_L}}\left(\frac{g\Theta_z}{\nu_L\kappa_L}\right)^{1/3}\right] \qquad \Theta_z < 0$$

$$\kappa = \nu_L \qquad \Theta_z > 0 \quad (4)$$

$$\kappa = \kappa_L \qquad \Theta_z > 0$$

The diffusivity and conductivity were divided into two parts, one was constant valued, while the other was a nonlinear part which depended on the local Rayleigh number when a locally unstable density region was present. This method was found to be very efficient for simulating the dissipation due to the breaking of internal gravity waves. Preliminary experiments showed that the spectra were relatively insensitive to a range of values for ν_{NL} and ν_L. The values chosen were such that when no wave breaking occurred, the system evolved inviscidly ($\nu_L = 10^{-5}$ cm^2/s); when overturning occurred, the eddy diffusivity attained a value consistent with measured values from the laboratory or field ($\nu_{NL} \sim 1$ cm^2/s).

3. Wave Interactions in a Continuous Spectrum

Numerical experiments were performed where energy was either given to individual modes or a band of wave numbers in a random background field of internal gravity waves, and the energy transfer from either the modes or bands to the rest of the spectrum was investigated. Six different experiments will be discussed in this section, and the pertinent information is given in Figure 2. In the first three experiments, called spike-random, energy was introduced at distinct modes of low, medium, and high wave numbers, while energy was placed in low, medium, and high wave number bands in the second three experiments. A description of the background random field will be presented before discussing the energy transfer experiments.

Random Internal Wave Field

The numerical model was integrated for a long duration ($1050T$), where T is the Brunt Vaisala period ($2\pi/N \simeq 8.3$ s). The random body forcing was introduced in space and time to the vorticity field. We can decompose the stream function ψ into Fourier components at any time t_i as follows:

$$\psi(x, z; t_i) = \sum\psi_{M,N} \sin\frac{M\pi x}{L} \sin\frac{N\pi z}{L} \quad (5)$$

where L and H are the container length and height, respectively, and the modes can be labeled (M, N). The total wave number k for a particular mode is given by

$$k^2 = \left(\frac{M\pi}{L}\right)^2 + \left(\frac{N\pi}{H}\right)^2 \quad (6)$$

The forcing was done by first randomly choosing a maximum horizontal and vertical wave number, M_m and N_m, respectively. The coefficients $\psi_{M,N}$ were then assigned random values from the gravest mode (1, 1) up to mode (M_m, N_m). This forcing was applied at the random times t_i, and the characteristics are shown in Table 1 for approximately a 2000 time step period. The first column of Table 1 shows the random times at which the forcing was applied, while the six columns show the number of modes forced (Table 1; notice that Fourier components with no x variation are possible ($I = 0$) but are not included in Figure 2.) The maximum amplitude of the forcing in vorticity was ~0.005 s^{-1}, which resulted in the build-up of a random field of internal gravity waves at all resolvable space and time scales. (The model resolves approximately 750 waves with a total of 3000 grid points, and approximately 150 waves are very well resolved (up to approximately (10, 15)). Most of the waves to band 5 in Table 1 are well resolved.) The spectral energy level increased monotonically in time until the combined effects of the small amount of random noise plus the existing finite amplitude waves produced localized overturning, which in turn, increased the overall eddy diffusivity and caused a reduction in the energy growth. From that point on, it became more and more difficult to increase the overall energy level, implying that a saturation level was reached for the model. We note that this does not mean all portions of the spectrum are saturated, and this is not a saturated spectrum.

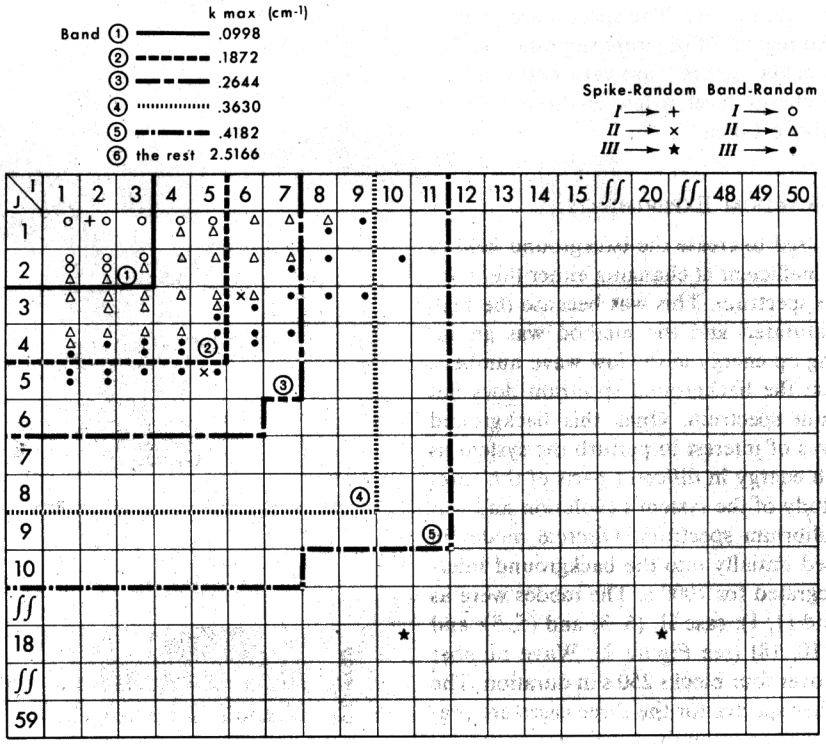

Fig. 2. Distribution of wave numbers (I, J) initially forced in the six different experiments. Note the distribution of wave numbers for each of the bands.

This question will be addressed in the subsequent series of experiments.

Frequency spectra for the horizontal and vertical kinetic energies ($|u_\omega|^2/2$, $|w_\omega|^2/2$) and potential energy ($g^2|\rho_\omega|^2/2N^2$) were computed from time series taken at different positions in the tank. The positions were C1(0.20L, 0.16H), C2(0.33L, 0.38H), C3(0.60L, 0.93H), and C4(0.81L, 0.50H), where the origin of the (x, z) coordinates is at the lower left-hand corner of the tank. The spectra were calculated from data blocks of 500-s duration (2000 time steps, or approximately 60T) with a total of 33 blocks ($\sim 7 \times 10^4$ time steps). The average spectra and the dispersion due to the individual spectra for the horizontal and vertical kinetic energies and the potential energy at position C2 are presented in Figure 3. Note that the vertical scale represents the energy (not the spectral energy density) at each frequency increment; the more standard representation of spectral energy density versus frequency on log-log scales will be presented later. The horizontal kinetic energy is shown in Figure 3*a*, and the slope is negative from low frequencies to N and falls with a steep slope beyond N. At first sight, the dispersion appears large, although one must remember that early data blocks enter into the dispersion when the energy level is still low, and the dispersion for the final 10 data blocks is very small. Small peaks can be observed superimposed on the background spectrum, but the field is not dominated by discrete modes. The average vertical kinetic energy is shown in Figure 3*b*, and the energy level increases with frequency until a maximum is reached near N, and then the energy abruptly falls off, a result consistent with the spectral shape for internal gravity waves. The average potential energy spectrum is given in Figure 3*c* and shows a shallow decreasing of energy as frequency increases up to N, and then falls rapidly. Inspection of the spectra shows that the sum of the horizontal and vertical kinetic energies will yield a spectral shape similar to the potential energy spectral shape, as might be expected from the equipartition of energy as applied to internal gravity waves.

This system of internal gravity waves is a fully nonlinear one, and the degree of wave breaking is substantial. In fact, energy contained in frequencies above N arises from either forced nonlinear oscillations or turbulence due to wave breaking. Even so, the relationships between the various spectral components and their shapes could be predicted by simple linear theory. The lack of discrete modes dominating the solution can be clearly observed in Figure 4, where the average potential energy spectra from the four positions, C1–C4, are presented. The similarity is striking, although some small peaks due to modes appear and are a function of position.

A measure of the stationarity of the random wave field energy can be seen in the wave number spectra corresponding to the last 1000 s of the experiment, which is presented in Figure 5. These wave number spectra were computed at every time step and then averaged over a block 250 s ($\sim 30T$) in duration. The spectra represent the energy at each wave number inter-

TABLE 1. Number of Modes Forced and Corresponding Random Times

Time of Random Input t_i	Wave Band					
	1	2	3	4	5	6
0	9	14	21	24	8	
429	8	2				
247	9	16	23	22	10	3
397	9	16	23	31	15	17
531	6	4	2			
130	8	8	7	1		
382	6	3				
2166	55	63	76	78	33	20

val, as opposed to a spectral density. The spectra are seen to be red in nature, and two regions of different slope can be discerned. Wave numbers below 0.6 cm^{-1} are very well resolved by the model, and the energy level is low at the poorly resolved wave numbers above 1.0 cm^{-1}.

4. Spike-Random Experiments

The random forcing used to create the background field of internal waves became inefficient at changing either the shape or the amplitude of the spectrum. This was because the high wave numbers were saturated and the method was an inefficient one for building up energy in the low wave numbers. It is for this reason that the background spectrum does not represent an equilibrium spectrum. Once this background field was obtained, it was of interest to perturb the system as an initial condition with energy in different parts of the spectrum. This allowed a study of the system's evolution and was used to create an equilibrium spectrum. Discrete modes in vorticity were introduced initially into the background internal wave field, and integrated for 1000 s. The modes were as follows: case I, (2, 1) and (1, 1); case II, (6, 3) and (5, 5); and case III, (20, 18) and (10, 18) (see Figure 2). Wave number spectra were computed over four blocks 250 s in duration. The total energy wave number spectra for the three cases are presented in Figure 6, and the arrows in the lower part of the figure mark the wave numbers at which energy was introduced. The salient features of the three experiments can now be described. Case I, block 1 (0–250 s) shows a large amount of energy in the wave number band containing (2, 1) with neighboring bands containing more energy than in the initial background spectrum. Note that in a short time of only $30T$ a significant amount of energy was transferred from (2, 1) to its neighboring wave numbers. In block 2 (250–500 s) this transfer to intermediate wave numbers is even more apparent, and as the principal triad components populate this wave number region, the effects of the previously discussed energy cycle are being observed. By block 4, the band containing (2, 1) regains some of its initial energy with the difference going to higher wave numbers, which show a net increase in energy. Dissipation due to wave breaking is occurring, and a decrease in the total energy from block 1 to block 4 can be observed.

Energy was introduced at intermediate wave numbers in case II. Peaks representing the modes (6, 3) and (5, 5) are evident in block 1 and a significant transfer of energy to lower wave numbers has occurred during this first interval. A decrease in energy from block 1 to block 4 occurs due to dissipation by wave breaking, and the greatest energy loss exists at intermediate wave numbers where both wave breaking and wave-wave transfers occur. Case III introduces energy at very high wave numbers, and any energy change is dominated by wave breaking, although a small degree of wave-wave interactions takes place. It should be pointed out that the input energy for these high wave number modes is relatively low; this is because the region is very close to saturation and it is difficult to introduce energy without causing a high degree of wave breaking.

A wave band analysis was performed to demonstrate the manner in which energy was distributed in wave number space. Six bands were chosen such that the first band contained modes of wave numbers ranging from the gravest to Δk, the second band contains waves from the gravest mode to $2\Delta k$, and so on, until the sixth band which contains the total

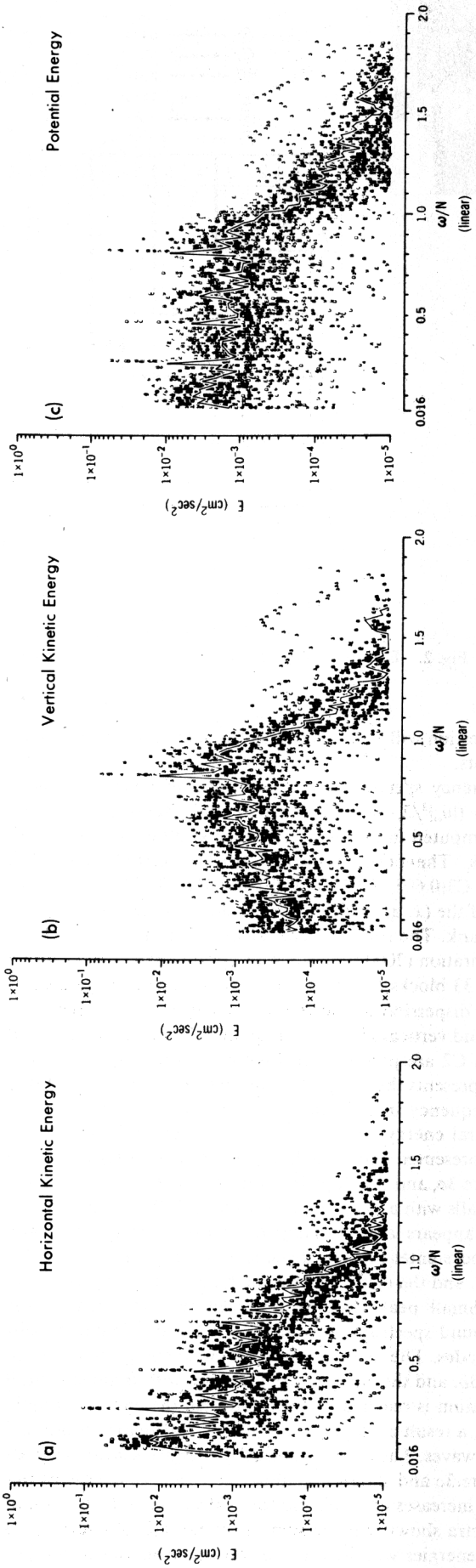

Fig. 3. The average spectra and the dispersion due to individual spectra for the horizontal and vertical kinetic energies ($|u_\omega|^2/2$, $|w_\omega|^2/2$) and the potential energy ($g^2|\rho_\omega|^2/2N^2$) are presented for the finite amplitude, random internal wave field. The probe position is ($0.33L$, $0.38H$).

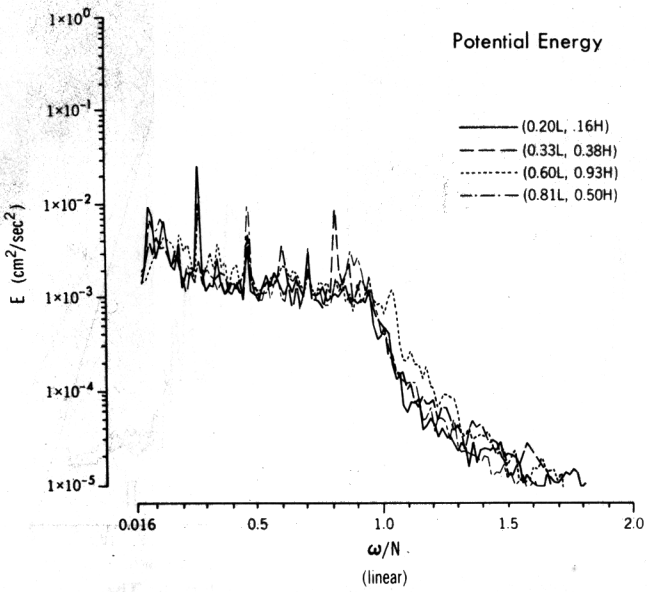

Fig. 4. The average potential energy spectra at four probe positions, (0.20*L*, 0.16*H*), (0.33*L*, 0.38*H*), (0.060*L*, 0.93*H*), and (0.81*L*, 0.50*H*), from the random internal wave field.

energy in all waves. Table 1 shows the band distribution, and results from this analysis are presented in Figure 7.

For case I, band 1 oscillates during the first 30*T*, indicating that wave-wave interactions are taking place. Energy is continually being pumped to the higher wave numbers as indicated by a relative increase in the difference between band 5 and band 6. After a short time (~60*T*), the oscillatory behavior ceases and the overall energy decreases, implying that dissipation by wave breaking is more important than wave-wave interactions in removing energy at each band. Case II shows a more direct cascade to higher wave numbers. Initially, bands 1 and 2 grow, indicating wave-wave transfers and a decascade of energy, but in a short time (less than 30*T*) a large amount of energy goes to high wave numbers, and dissipation via wave breaking occurs. In case III a small amount of energy was introduced by high wave numbers which are near saturation. No indication of wave-wave interactions appear, and the energy is slowly decaying due to wave breaking dissipation.

5. Band-Random Experiments

It is unquestionably realized that determining the energy transfer for internal waves in a realistic system requires the investigation of energy input over a band of wave numbers rather than at discrete modes. Three numerical experiments were conducted where energy was placed as follows: three numerical experiments were conducted where energy was placed in a low wave number band (case I), an intermediate wave number band (case II), and a high wave number band, case III (see Figure 2 for the initial wave components used in each experiment). The initial amount of energy placed in the wave number bands was approximately inversely proportional to the wave number. This is because the high wave numbers cannot sustain the same energy as the low wave numbers due to wave breaking. This initial energy is not an important factor in determining the final behavior and shape of the spectra.

Wave number spectra for the total energy are presented in Figure 8 for the band-random experiments. The format is similar to that of Figure 6, and the marked intervals in the lower portion of the figures show the band of wave numbers at which energy was introduced. In case I, a transfer of energy from low to intermediate wave numbers occurs within the first block (250 s), and energy fills the high wave numbers by the second block, while the energy at low and intermediate wave numbers decreases. A loss of total energy occurs over the entire spectrum due to dissipation resulting from wave breaking. Case II shows some initial transfer of energy from intermediate to low wave numbers, and the high wave numbers are now being fed energy directly and more rapidly than in case I. Following block 1, the overall energy level decreases due to wave breaking, and again some minor transfer of energy to the intermediate wave numbers occurs. In case III, where energy is placed at high wave numbers, a small degree of wave-wave transfer occurs in the first block, and then energy dissipates at all wave numbers due to wave breaking, as evidenced by an overall decrease in the energy level at all wave numbers. The spectral representation is not ideal for observing energy transfers but does show the characteristic slopes at various times during the experiment.

Notice that the spectral slope of the high wave numbers changed during and after intense wave breaking. For instance, during the time interval of intense breaking (block 2) in cases I–III the spectral slope is steeper than the slope at the last time interval (block 4), where light breaking was observed.

A better representation for observing energy transfers in wave number space is the wave band analysis shown in Figure 9, where the cumulative energy in each wave band is given as a function of time, similar to that shown in Figure 7. Case I is presented in Figure 9*a*. The energy initially contained in bands 1 and 2 is rapidly (~10*T*) distributed to other bands containing higher wave numbers. This cascade continues until approximately 30*T*, and most of the input energy is lost to ei-

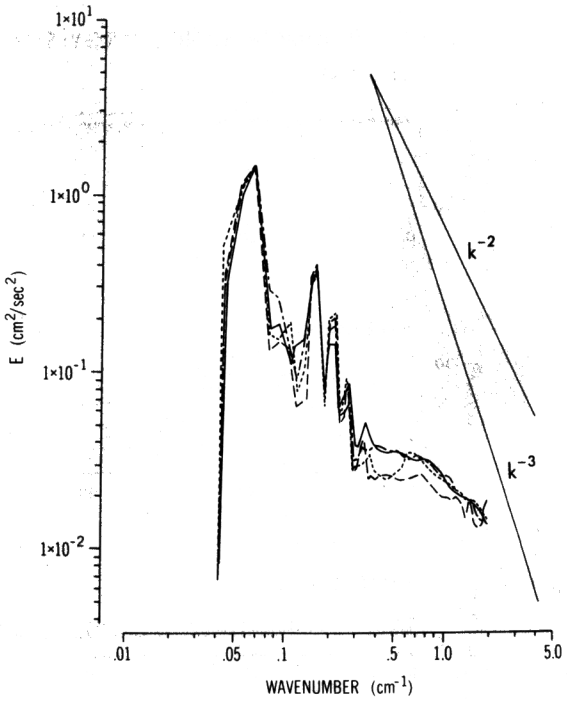

Fig. 5. Wave number spectra for the random internal wave field energy are presented for four consecutive time intervals following the build-up of the random wave field.

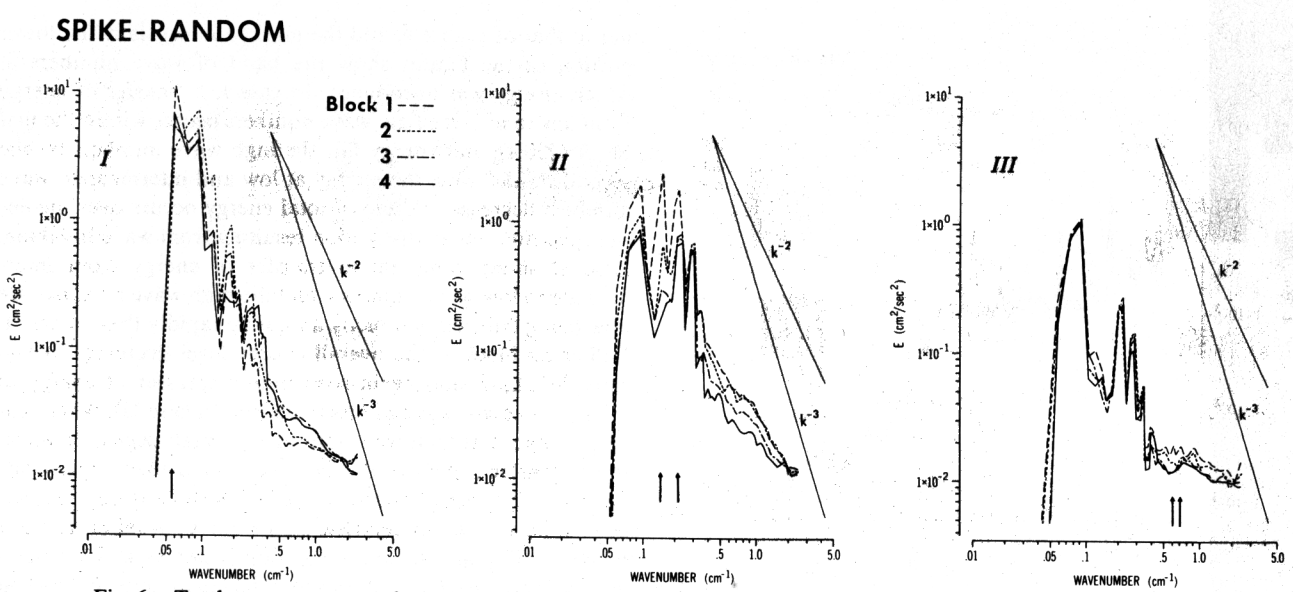

Fig. 6. Total energy wave number spectra from the spike-random experiments for four consecutive time intervals. The arrows mark the model wave number at which energy was introduced.

ther diffusion directly or has been transferred to high wave numbers. A very small degree of energy transfer back to band 1 occurs at $30T$, and the system is now predominantly losing energy via wave breaking. Case II, given in Figure 9*b*, shows a rapid (less than $10T$) energy loss of the intermediate wave band 3 to bands 2 and 6 predominantly, and band 1 to a lesser degree. In subsequent times, band 2 is losing energy to high wave numbers with the total energy (band 6) decaying due to breaking. One should note that the dissipation rate is band, or wave number, selective, where band 1 decreases slowly, while bands 4, 5, and 6 decrease much more rapidly with respect to time. Case III is presented in Figure 9*c*, where the energy input is at high wave numbers, and energy is transferred to higher wave numbers very rapidly with only a small amount of energy transfer to lower bands via wave-wave interactions. The common feature for all three experiments is the rapidity of the energy transfers, the pumping of energy to the high wave numbers, and the diffusion due to wave breaking.

The wave-wave interactions occur on a relatively short time scale of order $10T$ in all three experiments (questioning the

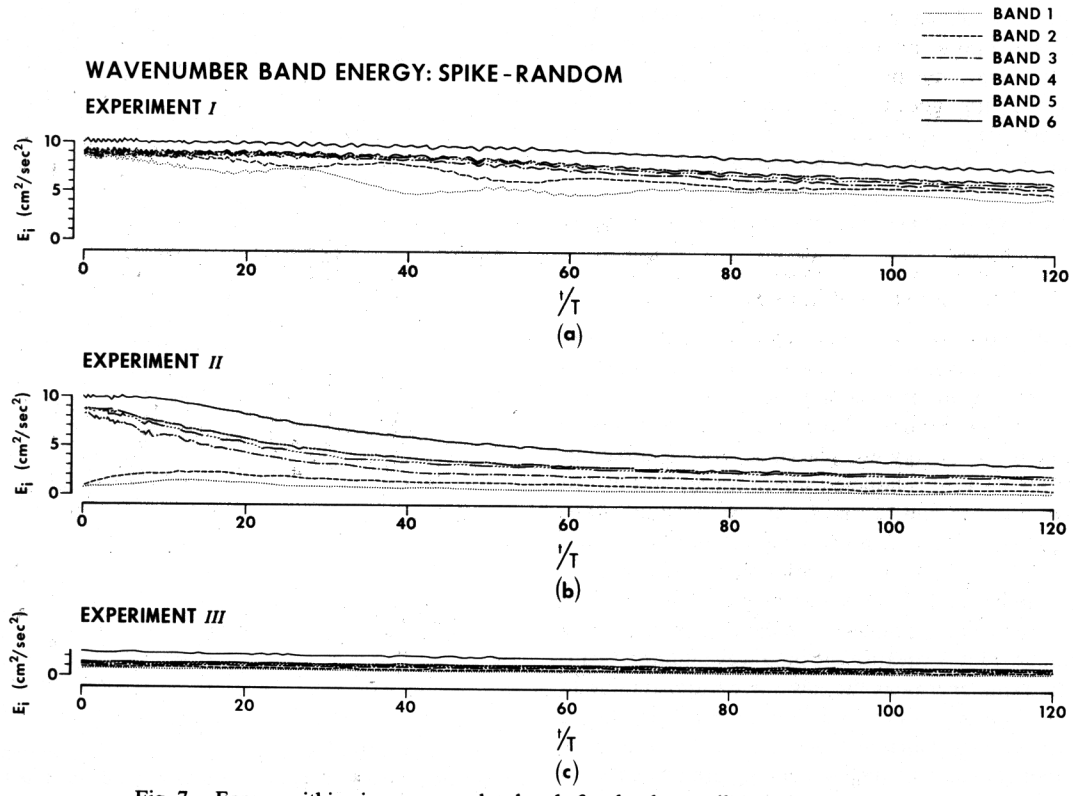

Fig. 7. Energy within six wave number bands for the three spike-random experiments.

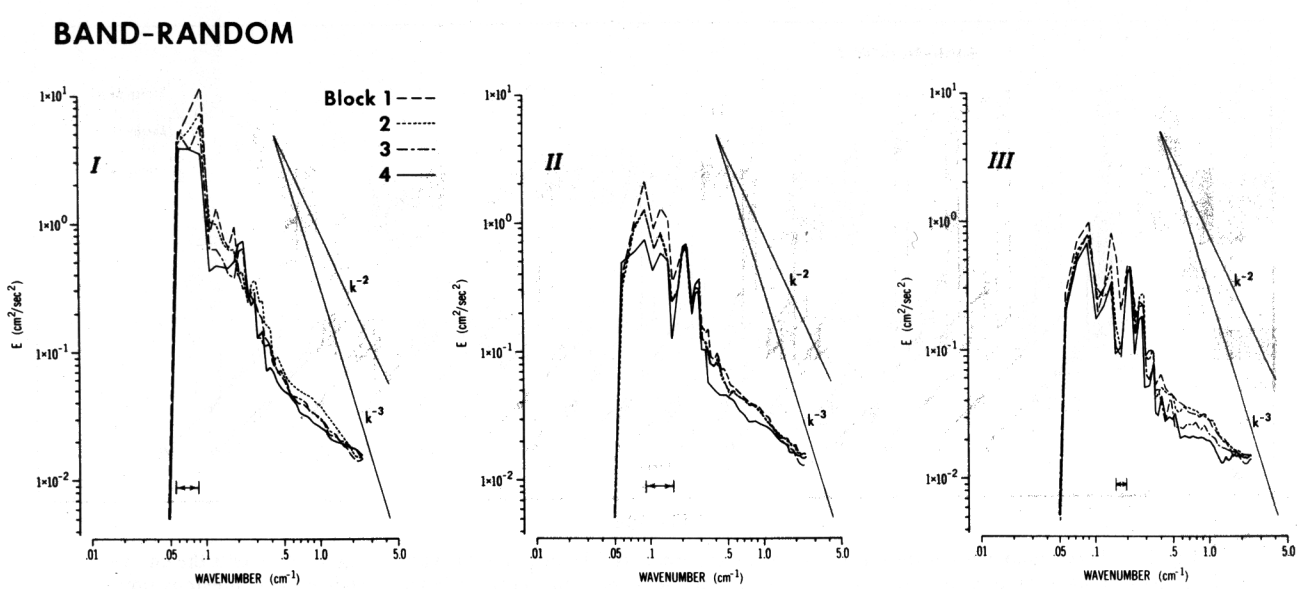

Fig. 8. Total energy wave number spectra from the band-random experiments for four consecutive time intervals. The marked intervals show the range of wave numbers at which energy was introduced.

validity of any weak interaction assumptions), and this time scale depends on the band energy levels. Diffusive time scales τ_i can be computed for the overall dissipation due to localized wave breaking, and they are as follows: case I, $\tau_I = 124T$; case II, $\tau_{II} = 104T$; and case III, $\tau_{III} = 168T$, where τ_i depends on the energy levels of the various bands. The eddy diffusivities for the gravest mode from the three cases can be estimated and are 0.50, 0.76, and 0.47 cm^2/s, respectively; these diffusivities agree remarkably well with the estimated oceanic values.

A more descriptive representation of this complicated, interacting system of internal gravity waves, where both wave-wave interactions and dissipation due to wave breaking are simultaneously occurring, is given in Figures 10*a*–10*c*. Case I of

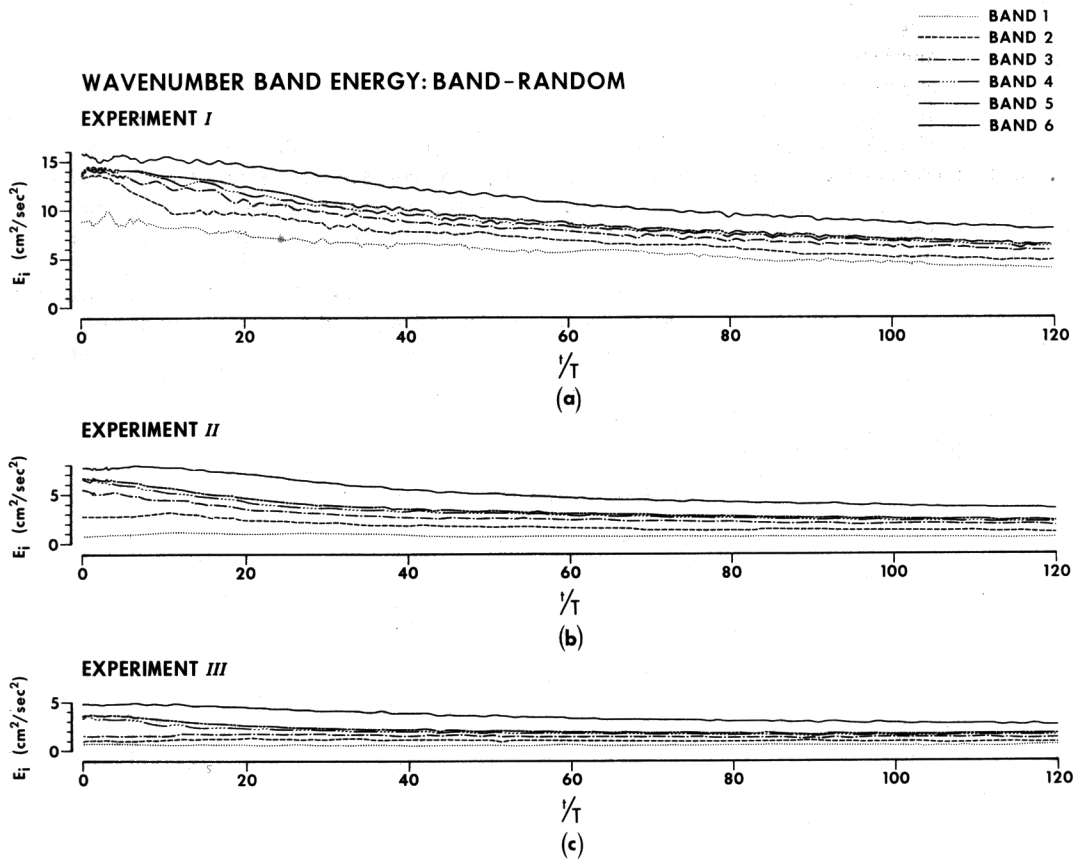

Fig. 9. Energy within six wave number bands for the three band-random experiments.

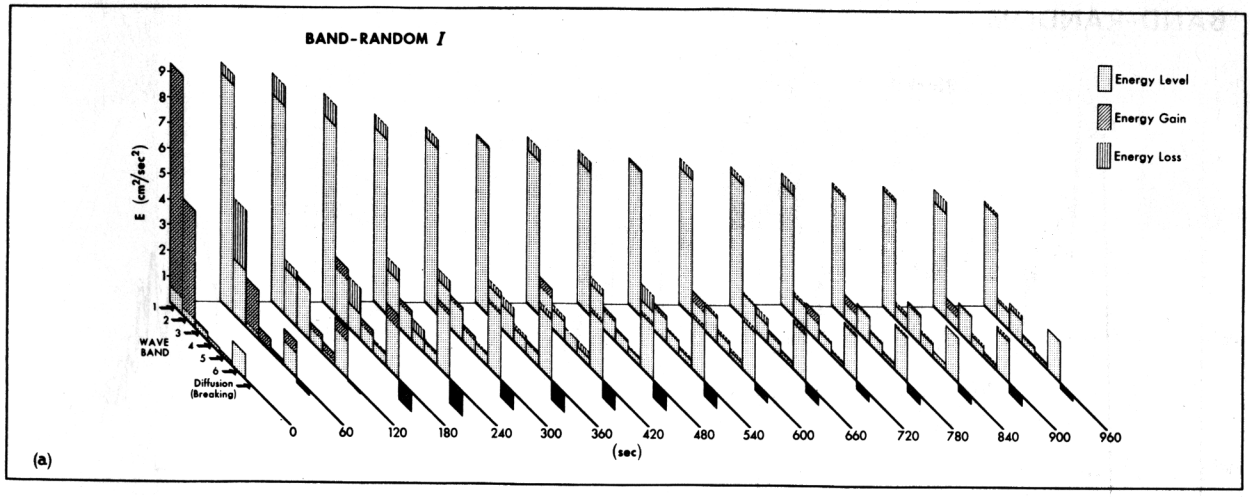

Fig. 10*a*

Fig. 10. Wave band analysis for the band-random experiments. The height of the vertical blocks represents the energy in each of six wave bands at the given time. The diagonal lines denote an increase of energy relative to the previous time, and the parallel lines denote a loss of energy. The seventh block, labeled diffusion, represents energy loss over all wave numbers due to wave breaking.

the band-random experiment is presented in Figure 10*a*, while cases II and III are shown in Figure 10*b* and 10*c*, respectively. Case I is shown for a duration of 960 s, while cases II and III are shown for 480 s, as by this time, diffusive processes outweigh wave-wave interactions and the time rate of change is very slow. The graphs depict the amount of energy in each band, in contrast to the cumulative band energy shown in Figures 7 and 9. The previous representation showed the energy contained in a band of wave numbers from K_0 to K_i, while the present representation shows the energy contained in an incremental band of wave numbers from K_i to K_{i+1}. The vertical scale is in energy units (cm^2/s^2), and the block height (stippled and drawn with a solid line) represents the energy contained in that band at the given time. The diagonal lines in the upper portion of the block represent an increase in band energy relative to the previous time (60 s), whereas the areas marked with parallel lines represent energy loss relative to the previous time (60 s). The seventh band represents energy loss over all wave numbers relative to the previous time, and this loss is due to wave breaking. Such a representation provides a clearer picture of energy transfers between bands due to wave-wave interactions and energy losses due to wave breaking.

Case I, Figure 10*a* shows the $t = 0$ background spectrum plus the additional energy placed in the lower bands 1 and 2. After a time of 60 s (less than $8T$), band 2 loses a large amount of its energy, while band 1 loses a smaller amount, and this loss goes into bands 3–6 in differing proportions with a small amount of wave breaking dissipation occurring. The time scale for various wave-wave interactions can be observed in this representation, where band 1 gradually loses energy until $t = 360$ s and then begins to regain energy, whereas band 2 loses energy until $t = 180$ s and then begins to regain energy. Band 3 receives most of its energy within 120 s and loses energy after $t = 180$ s. Band 6 reaches a maximum amplitude due to wave-wave transfers by $t = 180$ s, and from that time on, wave breaking becomes significant. The energy lost due to wave breaking is a substantial percentage of the energy transfer due to wave-wave interactions, but one cannot conclude that breaking is predominantly taking place in band 6. As a matter of fact, band 6 gains energy during the times 180 and 240 s when breaking and dissipation are intense. Wave-wave

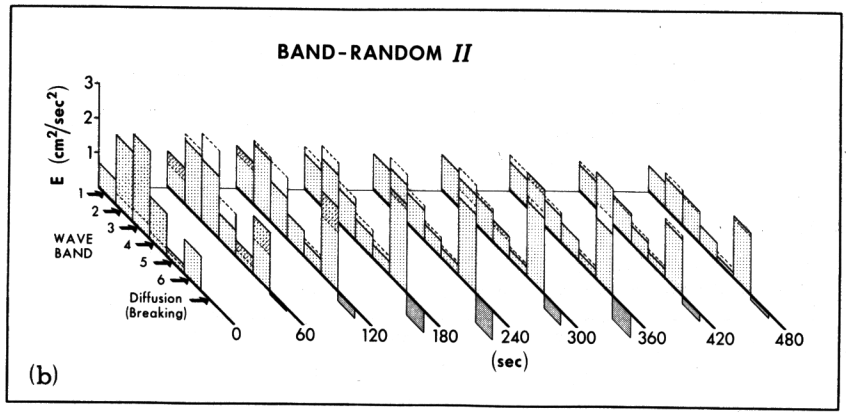

Fig. 10*b*

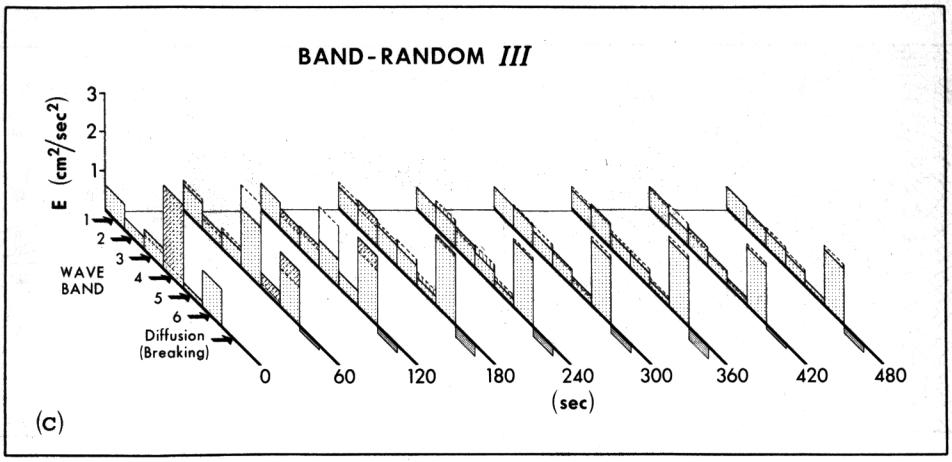

Fig. 10*c*

interactions and breaking continue throughout the experiment as the system slowly approaches an equilibrium spectrum.

Case II is presented in Figure 10*b* and during the first 120 s the cascade and decascade characteristic of wave-wave interactions is occurring within the low and intermediate wave bands. A considerable depletion of the input energy band occurs in a short period, followed by a period when wave breaking becomes an important factor in the energy loss for each band. Again, the system slowly approaches an equilibrium state. Case III is presented in Figure 10*c*, and the initial energy is predominantly in band 4. (Notice that Figure 2 shows initial perturbation ranges from band 2 to band 4, but band 4 contains the greatest energy.) Similar to the previous case, most of the wave-wave interactions occur in the first 120 s. It is interesting to note the transfers at different times, at $t = 60$ s, band 4 transfers energy to bands 5 and 6, while at $t = 120$ s, bands 2 and 3 are gaining energy. Again, energy loss due to wave breaking represents a significant percentage of the overall energy transfer.

We conclude from these results that wave bands 4, 5, and 6 become saturated by time 480 s, and inspection of the three experiments shows that the amplitude of these bands remains similar. We can also conclude that the equilibrium amplitude for wave band 3 is given at its final state of cases I and II. Results for wave bands 1 and 2 are inconclusive, but it appears that the amplitudes finally reached in case I represent approximate equilibrium values.

It is not implied that further energy input to any band will produce instantaneous breaking, but what is implied is that further energy input may be rapidly transferred by wave-wave interactions to higher wave numbers where breaking becomes likely. Such a cascade of energy, however, is not necessary for breaking, as the high wave numbers are near saturation and are superimposed on the lower wave numbers in physical space. Figures 11*a*–11*c* show streamline contours for cases I–III, respectively, at four different times. Regions in the flow field where the local eddy viscosity is nonzero due to overturning are indicated with blocks described in the legend. These regions are shown only on the right of each figure (unshaded area). In case I, we find a high degree of overturning soon after the additional energy input. A subsequent reduction in overturning occurs as the system evolves, and this is consistent with the evolution described in Figure 10. The results are similar for cases II and III, where at times soon after the energy input, a high degree of overturning exists. This wave breaking continues until the energy in each wave band is low enough, and the superposition of the waves rarely produces a situation in physical space where overturning can occur. This superposition means that any additional energy input to the low wave number modes can result directly in wave breaking. This implies that the amplitude of a single wave is a sufficient criterion for overturning, but not a necessary one. In fact, the collective contribution of all waves at a single position in physical space determines the conditions for breaking in a full spectrum. This point is relevant to the discussions of *Frankignoul* [1972] and *Garrett and Munk* [1972*b*], where the criterion for a single wave or band of waves was considered without treating the background contributions arising from low-frequency, low wave number oscillations. In the case of overturning, the criterion developed by *Orlanski and Bryan* [1969] involved the comparison of an exchange velocity (the time derivative of the density divided by the horizontal derivative of the density) to the advection velocity. The exchange velocity equals the phase velocity only for a single wave, and in this case, overturning occurs when the advection velocity exceeds the phase velocity. The criterion of advection velocity exceeding exchange velocity, on the other hand, can be used in the full spectrum case provided that the quantities represent contributions from all waves. In the case of shear instability, the Richardson number criterion discussed by *Phillips* [1966] must account for the collective values of wave shear and density gradient. A related conclusion which can also be drawn from the numerical experiments is that although the final amplitude for each wave individually was small, the collective nature of the wave field yields a system in equilibrium. The small amplitude for individual waves in this saturated spectrum resulted in linear relationships for the kinematical wave properties, but the wave field became very nonlinear when additional energy was introduced.

6. Energy Budget

The net amount of energy lost or gained at each band is shown in Figures 10*a*–10*c* and gives a clear description of the transient evolution of the energy input at different bands, where the final energy sink is dissipation due to overturning. Neither the amount of dissipation of each wave number or wave band nor the amount of gain or losses of energy by wave interaction can be determined from the previous results. It

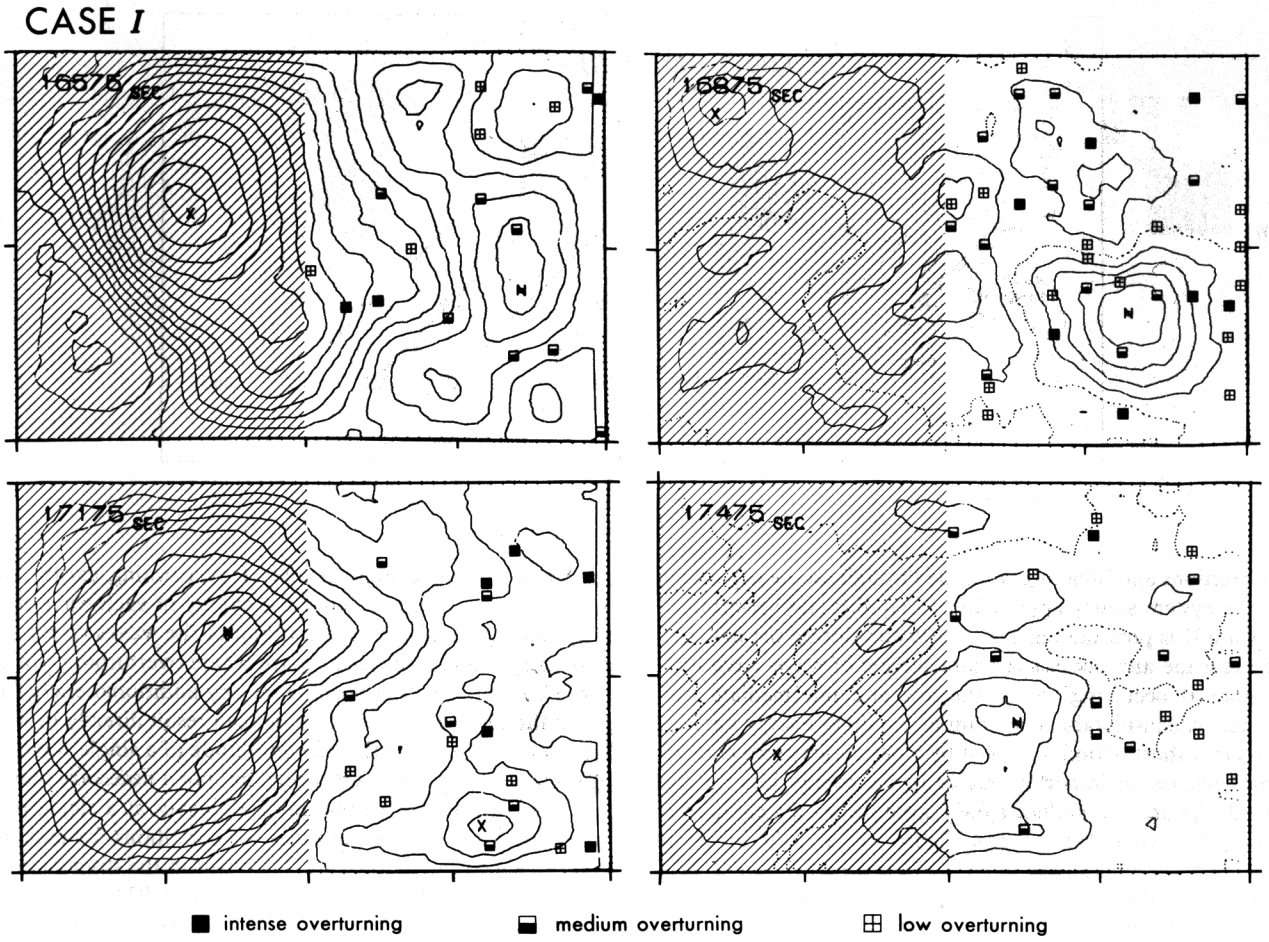

Fig. 11*a*.

Fig. 11. The contours of stream function at four different times are shown. Blocks indicate severity of local mixing due to wave breaking. The shaded region indicates that only half of the domain is wave breaking.

will be very important to understand and evaluate the amount of energy transfer by wave interaction and the loss by dissipation for each wave number in the spectrum. The energy balance equation for each Fourier component can be derived by making use of equations (1)–(3):

$$[(\nabla\psi)_t]_{MN} - [J(\psi, \nabla^2\psi)]_{MN} = [g\theta_x]_{MN}\ [\nabla\nu\ \nabla\zeta]_{MN} \tag{7}$$

$$[\theta_t]_{MN} - [J(\psi, \theta)]_{MN} = [\beta\psi_x]_{MN} + [\nabla k\ \nabla\theta]_{MN} \tag{8}$$

Multiplying (7) by minus the Fourier component of $\psi(-\psi_{MN})$ and (8) by $(-(g/\beta)\ \theta_{MN})$ integrating over the whole domain and making use of the boundary conditions, the equation of the energy budget is given by

$$\overset{\text{total energy}}{\frac{1}{2}\left\{\left(\frac{M\pi}{L}\right)^2 + \left(\frac{\pi}{H}\right)^2 |\psi_{MN}|^2 + \frac{g}{|\beta|}|\theta_{MN}|^2\right\}_t}$$

$$= \overset{\text{NLI}}{-\psi_{MN}\,[J(\psi, \nabla^2\psi)]_{MN} + \frac{g\theta}{\beta}{}_{MN}[J(\psi, \theta)]_{MN}}$$

$$\overset{\text{diss}}{- \psi_{MN}[\nabla\nu\nabla\zeta]_{MN} + \frac{g}{\beta}\theta_{MN}\,[\nabla\kappa\nabla\theta]_{MN}} \tag{9}$$

appropriate summation over the horizontal and vertical wave numbers (M and N) give the energy budget at each total wave number (k).

$$E_{kt} = (\text{NLI})_k + (\text{diss})_k \tag{10}$$

where the energy is given by

$$E_k = \frac{1}{2}\sum_M \sum_{N(M,k)} \left[\left(\frac{M\pi}{L}\right)^2 + \left(\frac{N\pi}{H}\right)^2\right] |\psi_{MN}|^2 + \frac{g}{\beta}|\theta_{MN}|^2 \tag{11}$$

The NL interact

$$(\text{NLI})_k = \sum_M \sum_{N(M,k)} -\psi_{MN}[J(\psi, \zeta)]_{MN} + \frac{g\theta}{\beta}{}_{MN}[J(\psi, \theta)]_{MN} \tag{12}$$

and the dissipation

$$(\text{diss})_k = \sum_M \sum_{N(M,k)} -\psi_{MN}[\nabla\nu\nabla\zeta]_{MN} + \frac{g}{\beta}\,\theta_{MN}\,[\nabla\kappa\nabla\theta]_{MN} \tag{13}$$

The quantities $(\text{NLI})_k$ and $(\text{diss})_k$ were numerically computed and integrated over time for the three band-random experiments. Results are presented in Figures 12*a*–12*c*, where the time integration extended over 250 s and corresponded to block 2 of data (as shown in Figure 8). Results from experiment I are presented in Figure 12*a*, where large negative values occur for $(\text{NLI})_k$ at wave numbers of approximately 0.15

CASE *II*

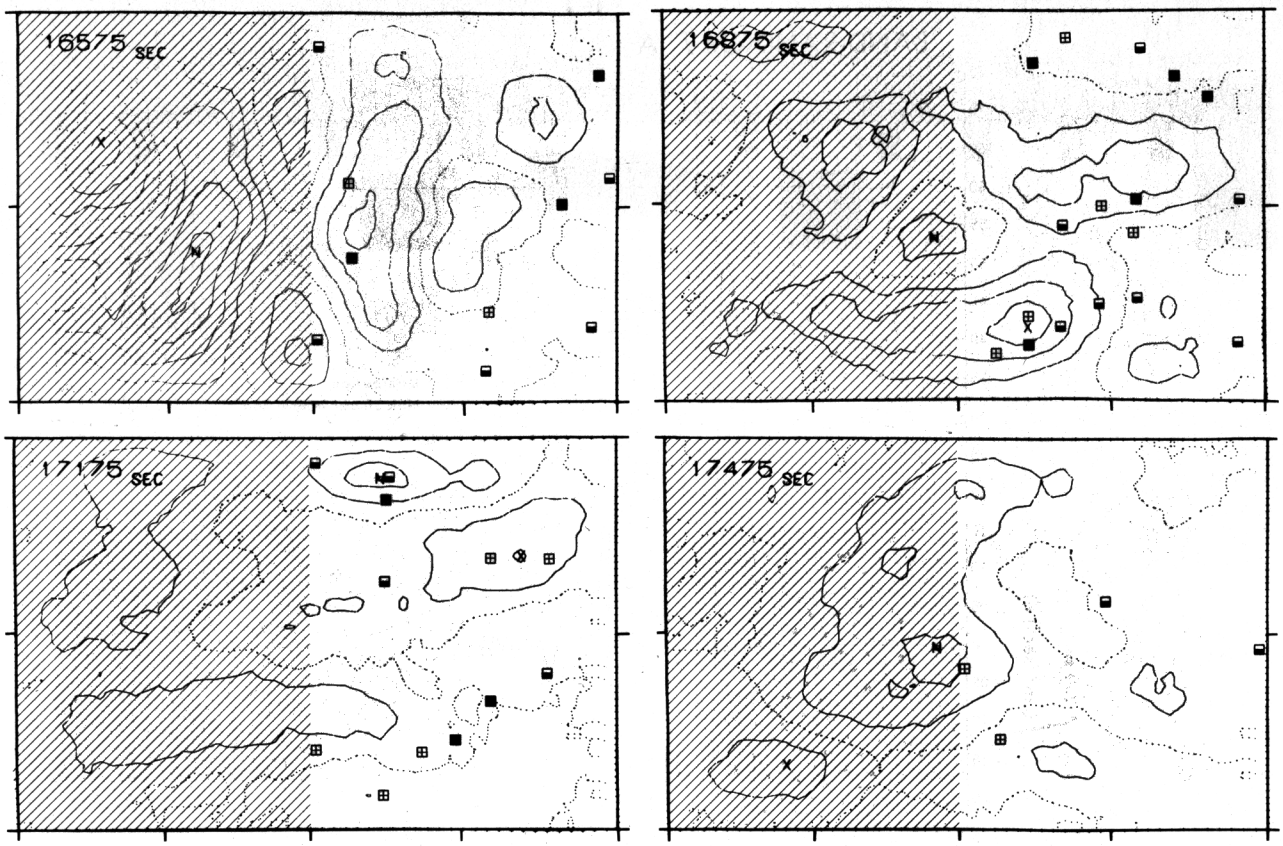

Fig. 11*b*.

CASE *III*

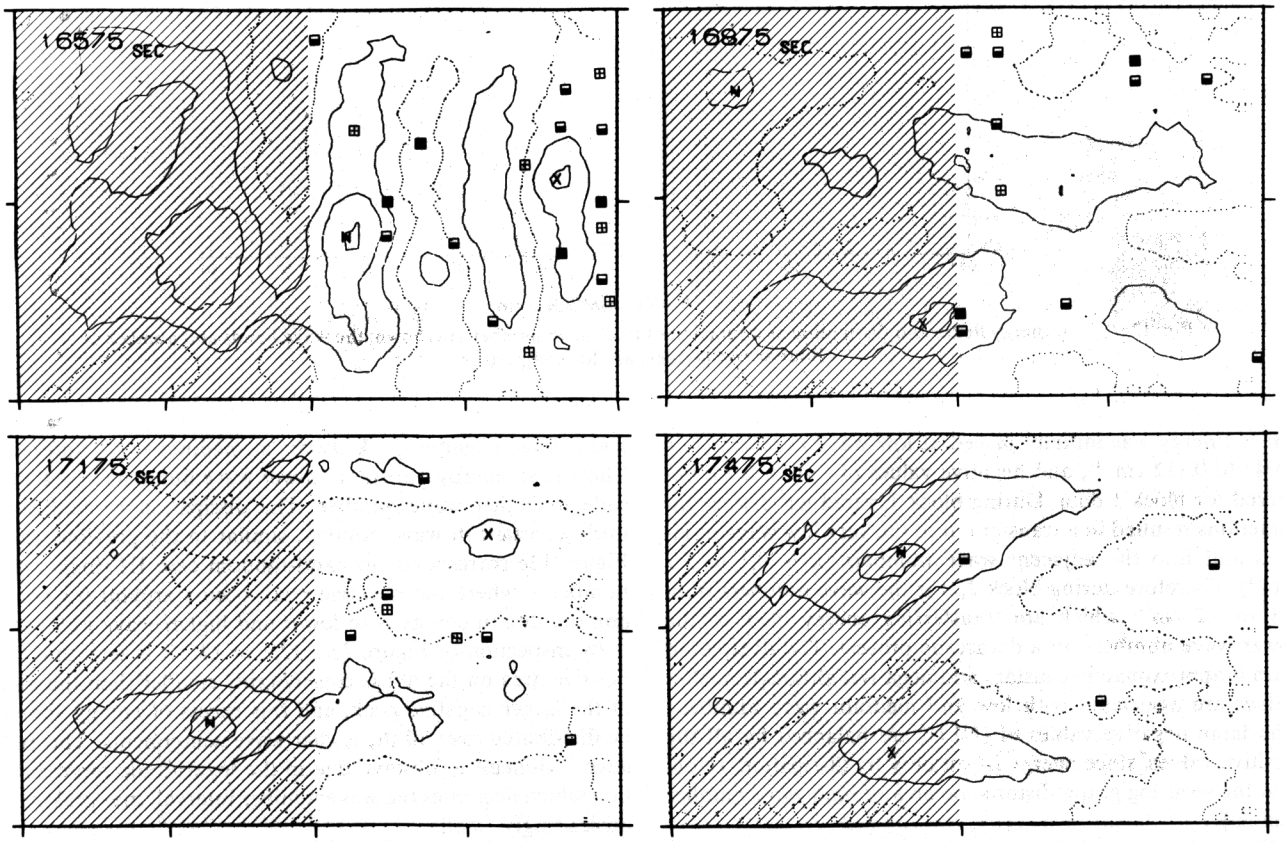

Fig. 11*c*.

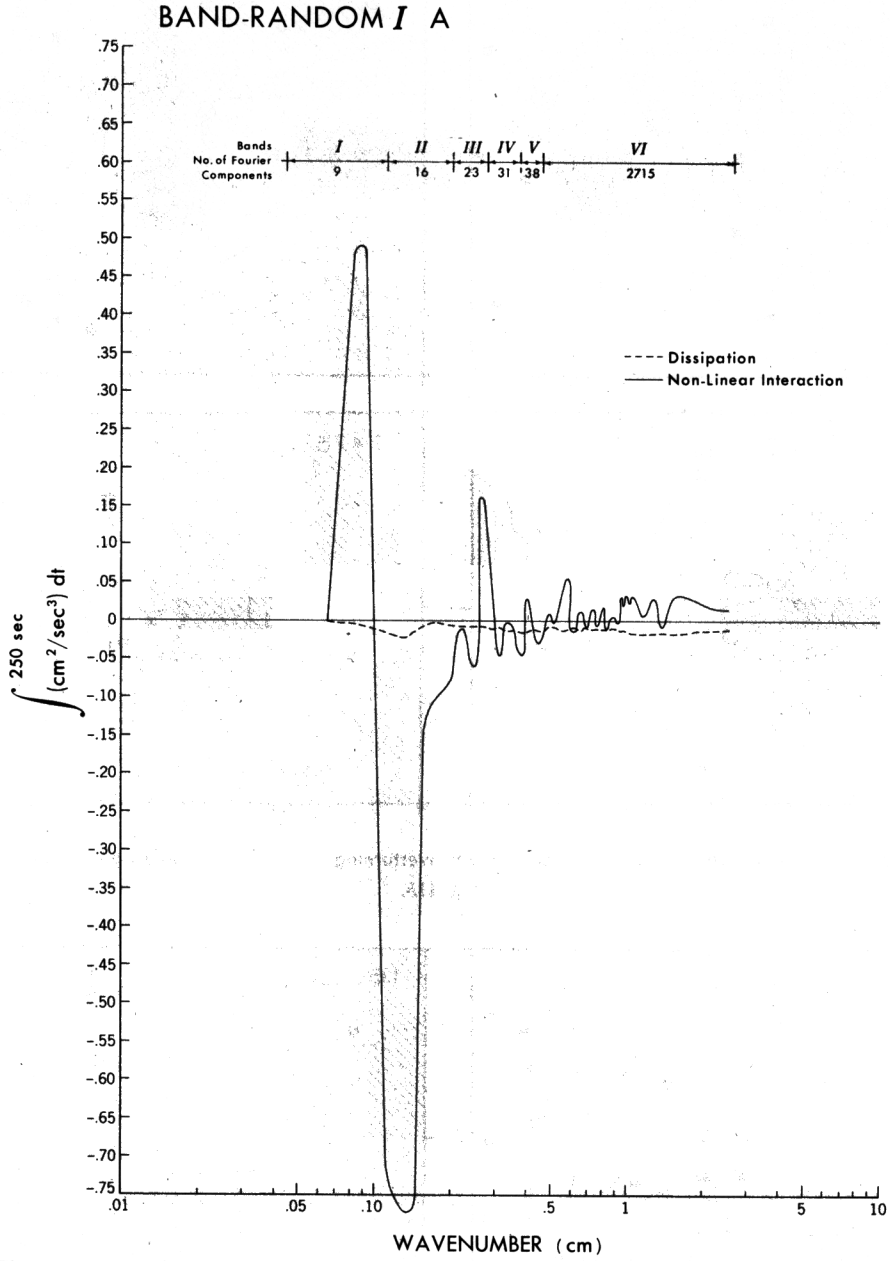

Fig. 12*a*. The energy fluxes and dissipation as a function of total wave number are shown; the wave bands and number of Fourier components are for comparison.

cm^{-1}. Energy was initially placed at low wave numbers (k = 0.043 to 0.112 cm^{-1}), and negative values of $(NLI)_k$ were observed for block 1 data. During block 1, rapid wave-wave interactions resulted in a transfer out of the very low wave numbers and into the adjacent wave numbers ($k \sim 0.1$ to 0.2 cm^{-1}). Therefore during block 2, it is the wave numbers from 0.1 to 0.2 cm^{-1} which are transferring energy back to the lower wave numbers, in a decascade process. The dissipation term is approximately constant and negative, although smaller values are associated with low and medium wave numbers. The large negative values of $(NLI)_k$ are balanced by all the positive values, since energy is lost only by dissipation. (Note that the semi-log graph distorts the area of high wave number region.)

Figure 12*b* represents the energy exchange for experiment II, where the input of energy corresponds to medium waves, and a large negative peak occurs at medium wave numbers. There is an energy transfer to lower wave numbers and a cascade to higher wave number. The dissipation is small and fairly constant in wave number, similar to the previous case. Figure 12*c* corresponds to band-random case III (high wave numbers), where the negative peak occurs around 0.3 cm^{-1}, and the flux of energy is to lower and higher wave numbers.

By inspection of Figure 12*a*, 12*b*, or 12*c*, it is seen that the positive area on the left is considerably smaller than the area of the larger negative peak, and this excess of energy should be distributed over all the higher wave components. This balance is difficult to observe due to the logarithmic representation which decreases the wave number interval, thus making it misleadingly small.

A clearer representation of the energy fluxes between bands is presented in Figure 13, where only the first $40T$ (320 s) are

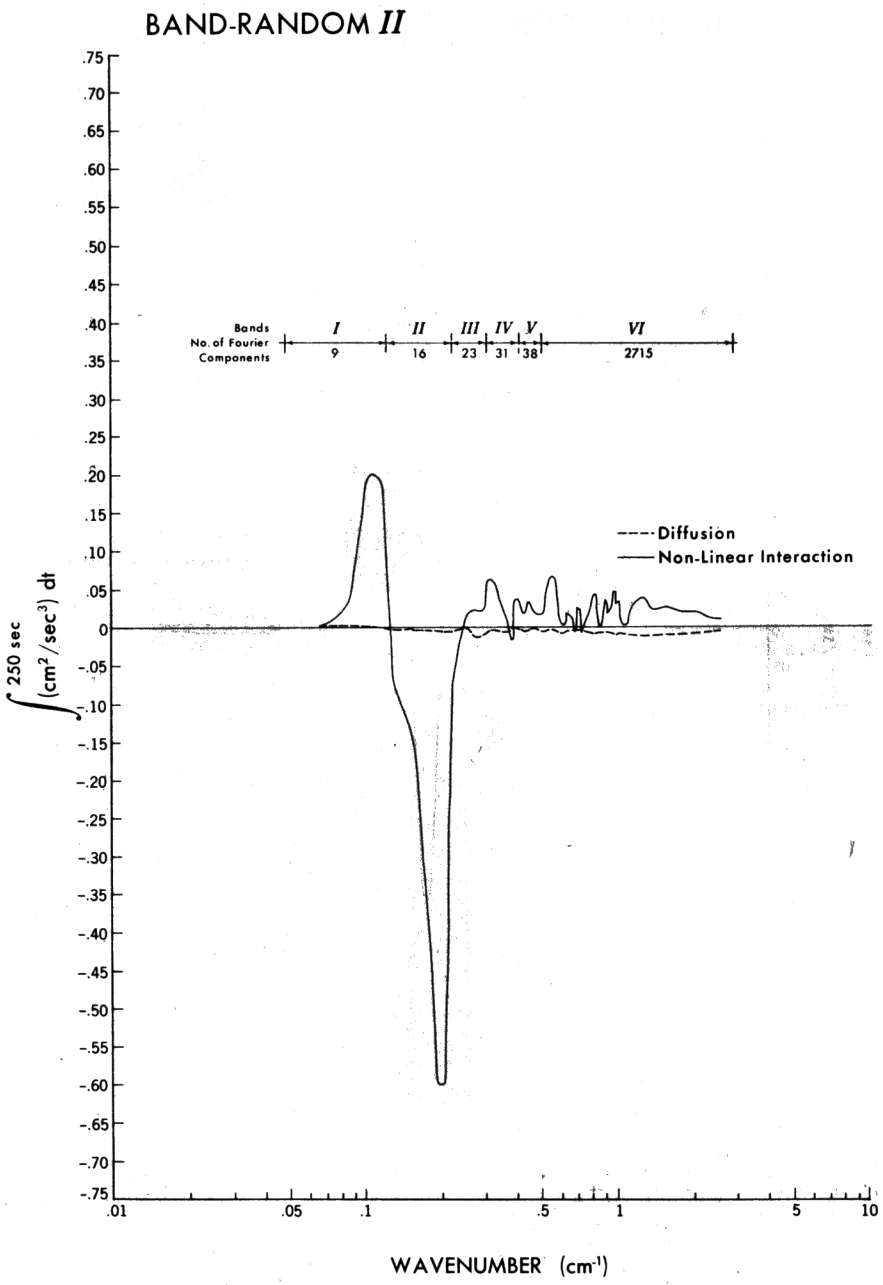

Fig. 12*b*. The same as Figure 12*a* but for case II.

presented. Each curve represents the sum over k for

$$\sum_{k_i}^{k_i+k} (\text{NLI}) \qquad \sum_{k_i}^{k_i+k} (\text{diss})$$

where the incremental wave number bands are defined in Table 1. Figure 13 depicts the process of energy transfer in the experiment and shows the fluxes (upper) and dissipation (lower) of energy at each band for the band-random case I experiment. During the first $20T$, energy in bands 1 and 2 decreases, while all other bands show an increase in energy (consistent with Figure 10*a*). The noteworthy feature is the constant increment of energy flux to high wave numbers (band 6). This occurs to such a large degree, that after $20T$ virtually all of the energy loss in bands 1 and 2 goes to band 6. Accordingly, there is an equivalent amount of energy lost by dissipation of the high wave numbers (band 6) and negligible at the other bands.

A consistent picture of the energy transfer for internal waves above the equilibrium can be constructed from the previous results (Figures 12 and 13). Wave-wave interactions mainly contribute to energy transfer between similar total wave numbers, that is, wave-wave interactions are local interactions in wave number space. Energy fluxes between different scales are mostly controlled by the strong interaction of very short waves with long and medium wavelength modes, where localized overturning and dissipation will occur at the small scales when excess energy is introduced. As previously stated, the energy need not pass through all intermediate scales but can directly go to high wave numbers due to overturning.

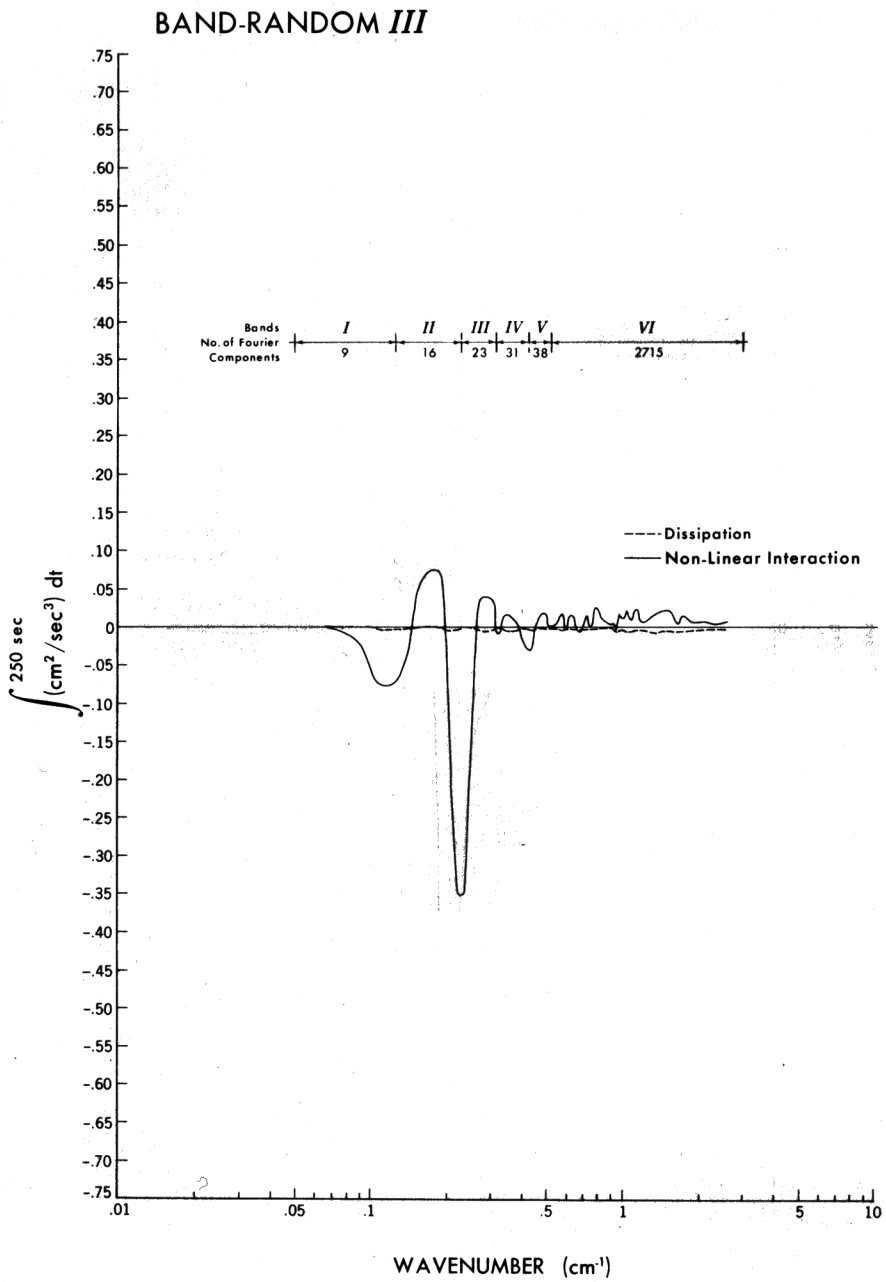

Fig. 12*c*. The same as Figure 12*a* but for case III.

The dissipation rate is approximately constant as a function of total wave number (Figure 14). The deviations from a constant value are related to the 'spikes' in the energy spectrum, and one can define a simple distribution function by dividing dissipation by the energy spectrum,

$$F(k) = \frac{\text{diss}(k)}{E(k)} \sim k^{5/2} \tag{14}$$

This quantity is then much smoother than diss(k) or $E(k)$ taken separately and obeys an approximate 5/2 power law.

One should notice, however, that to parameterize the dissipation by the formula given in (14) will require the explicit nonlinear interaction to higher wave numbers by overturning since these waves are the major contribution to the total dissipation. Spectral models where only weak interactions are simulated with be unable to reproduce the large fluxes to higher wave numbers which are required for effective dissipation. For such models a complete parameterization of the nonlinear strong interaction to higher wave numbers and the dissipation of (14) should be included.

7. Perturbations of the Equilibrium Spectrum

It was suggested in the previous section that the final state in band-random case I was an equilibrium spectrum (as opposed to a background field). The background spectrum was one in which the high wave numbers were saturated but the low waves were certainly not. Energy was introduced at low wave numbers in case I (spike-random or band-random) and the long time field appeared to be an equilibrium one where high wave numbers are saturated. This hypothesis was tested

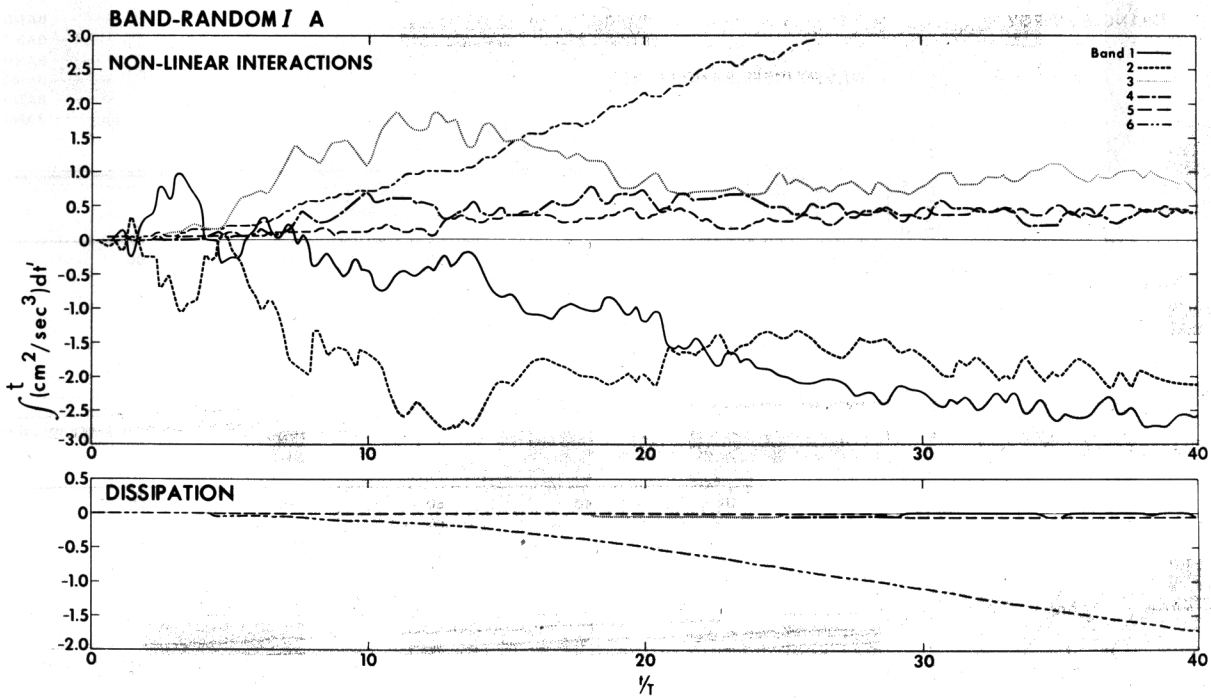

Fig. 13. The time integral of the energy fluxes (upper) and dissipation (lower) for each band of case I.

by again introducing energy at low wave numbers to the final state of experiment I. Before discussing those results, let us compare this solution with the evolution of low wave numbers in two other examples to illustrate the different behavior of the nonlinear interactions.

The two low wave number modes chosen were those of a resonantly interacting triad similar to the spike-random experiment given in case I of section 4. The evolution of the triad was studied in three situations: (1) the triad evolves without the presence of a background field, (2) the triad evolves in the presence of the random, small-amplitude background field of internal waves (spike-random case I), and (3) the triad evolves in the presence of the finite amplitude spectrum taken from the final state of band-random case I. The evolution of the triad in the absence of any background field is initally similar to that predicted by the solutions to the gyroscopic equations [*Orlanski and Cerasoli,* 1979]. Multiple triad interaction eventually excites modes other than the primary triad components, making the evolution more complex than that predicted by the gyroscopic solutions. Given its initial behavior of this system, we refer to it as the gyroscopic regime. The triad evolution in the second example is referred to as the Hasselmann regime. This title is chosen, as the system appears to have the characteristics necessary to use Hasselmann's formalism (small amplitude, random, and Gaussian). We do emphasize that once wave breaking becomes as important as triad interactions, Hesselmann's theory will not be valid. The final case is referred to as the strong interaction regime, where the triad is evolving in a finite amplitude field of internal waves.

Results from the three cases, gyroscopic, Hasselmann, and strong interaction regime, respectively, are presented in Figure 15. The energy band analysis is situated on the right of the figure, and a thin solid line at the initial energy level is included to better observe the total energy decay. The left side of the figure contains a triangle representation which is useful for describing triad evolution and is discussed by *Orlanski and Cerasoli* [1979]. The total energy in all components allows one to subdivide the energy into the energy of any two waves plus the rest. If no breaking occurs, the sum of these three energies will be conserved (neglecting the very small laminar viscosity). The time evolution of these three energies can be graphically presented as a curve inside an isosceles triangle, where the height represents the total energy. A point along the curve has the property that sum of the distance to each side of the triangle is equal to the total height. Therefore the distance to

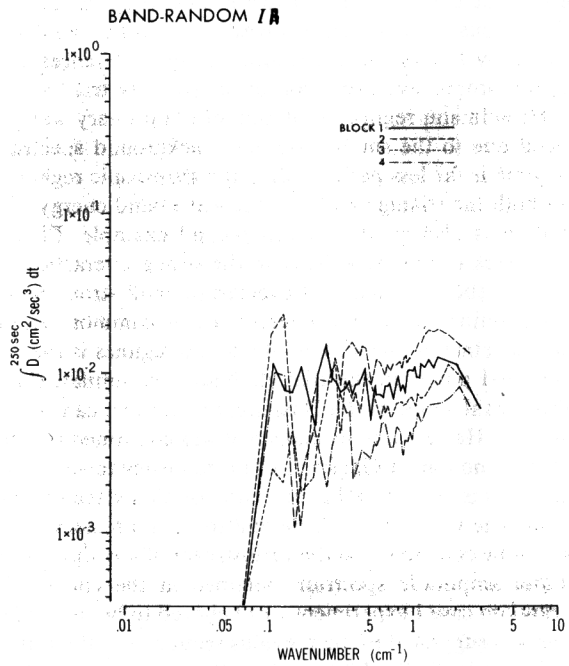

Fig. 14. The time integration of the dissipation versus total wave number for the Fourier time intervals of experiment I.

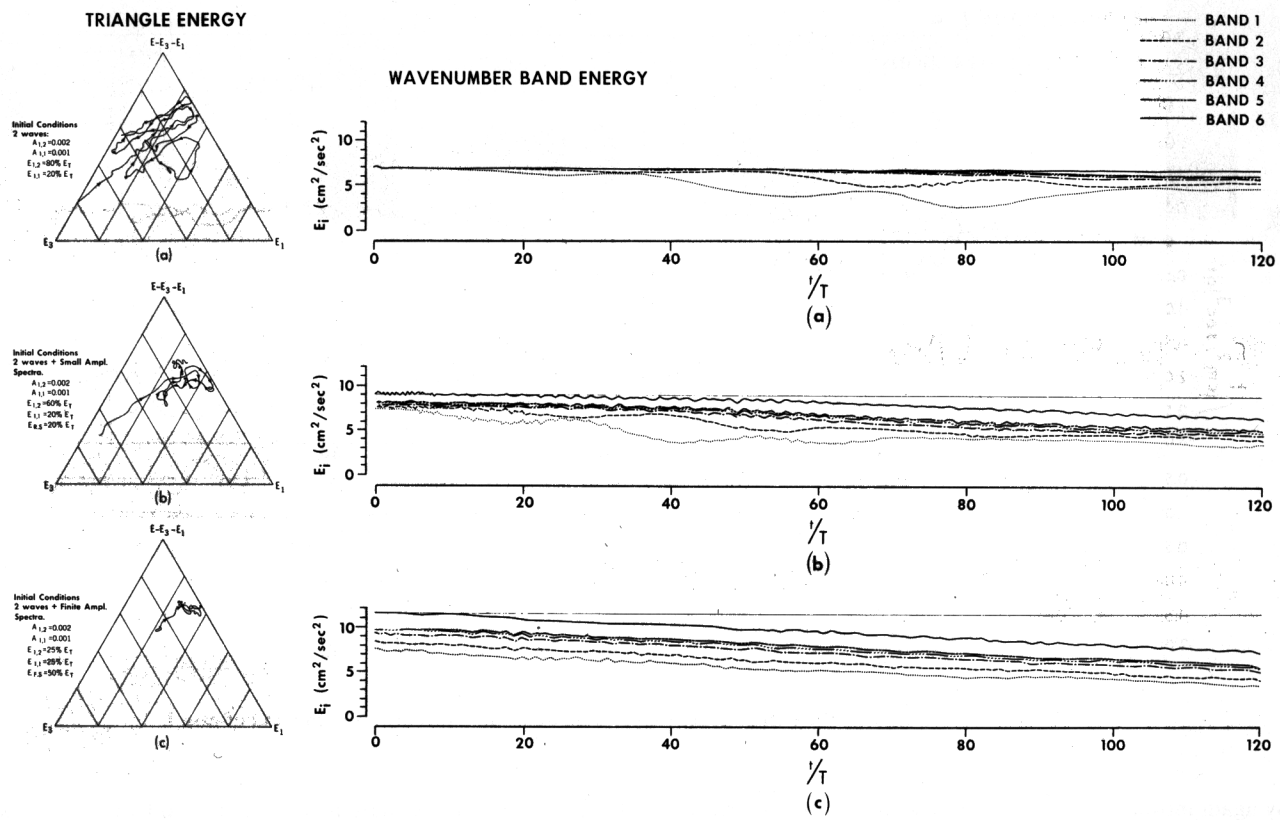

Fig. 15. Energy evolution in the triangle space (see text) is shown on the left and the energy of the different wave bands as a function of time on the right. Parts *a*, *b*, and *c* correspond to the single triad input, to the single triad plus background spectrum, and the triad plus the equilibrium spectrum, respectively. Notice that $E(1,1) = E_1$ and $E(1,2) = E_3$.

each side represents the energy. Three limiting cases are that (1) E_1 has total energy, (2) E_2 has total energy, and (3) $E_1E_2 = 0$, the rest of the modes have the total energy. These three cases correspond to points on the three respective vertices.

The triangle figure for the gyroscopic regime shows approximate straight lines for the first few evolutionary periods. As stated previously the system evolves in a manner similar to that given by the gyroscopic solutions, and differences exist due to the progressive excitation of nonprimary triad waves. In the Hasselmann regime, excitation of nonprimary waves is enhanced due to the small-amplitude background spectrum. This regime is far less periodic than the gyroscopic regime as seen in both the triangle plot and the wave band energy plot. Dissipation is also greater in this second example. Finally, there is a lack of any periodicity in the strong interaction regime due to the dominance of overturning and strong wave-wave interactions over triad interactions. A common feature for the Hasselmann and strong interaction regimes is the fact that the final points in the triangle figure are similar. (Note that these final states of the Hasselmann regimen can not be described by Hasselmann formalism; it was confirmed that the wave field is no longer Gaussian.) This tendency toward similar end states is related to the saturation of high wave number bands and the wave breaking present in such a system.

Let us now come back to the mainstream of our discussion. The finite amplitude spectrum obtained at the end of the band-random case I experiment was believed to be in equilibrium, as was suggested in the previous section. A similar analysis as shown in Figure 10*a* was done for this new case where a perturbation was introduced to the equilibrium state. Results are shown in Figure 16. In the first 60 s the energy lost by wave band 1 is balanced by dissipation due to wave breaking. The high wave number bands change very little, since they are saturated. It is interesting to contrast the evolution of this case with that of case I in Figure 10*a*. It was mentioned before that substantial changes in neighboring bands were observed in case I for the first 180 s due to wave-wave interaction and wave breaking with dissipation occurring after that. In this sensitivity study, the change in band energy level is less noticeable than in case I, implying that wave-wave interactions are not as predominant as in case I. On the other hand, wave breaking is activated far sooner, as can be seen by the fact that the energy lost in the first band is approximately equal to the energy removed by diffusion due to wave breaking (band 7). The final spectrum at $t = 960$ s is still decaying, and previous experiments suggest that this will continue until the equilibrium levels are achieved. One should note that the spectral shape changes very little.

Similar to Figure 13, Figure 17 shows NLI and diss for the final experiment. It should be noticed that the negative fluxes at the lower wave band are exclusively balanced by the fluxes at the higher band 6 with a compensatory loss due to dissipation. The result again seems to confirm that a spectrum can be in equilibrium (minimum loss of energy by dissipation due to overturning) if not perturbed, but efficient cascading to short waves and dissipation will occur if energy is introduced at any scale.

Throughout this paper, we have purposely avoided comparing our two-dimensional results for internal gravity waves with the three-dimensional oceanic counterparts. This was be-

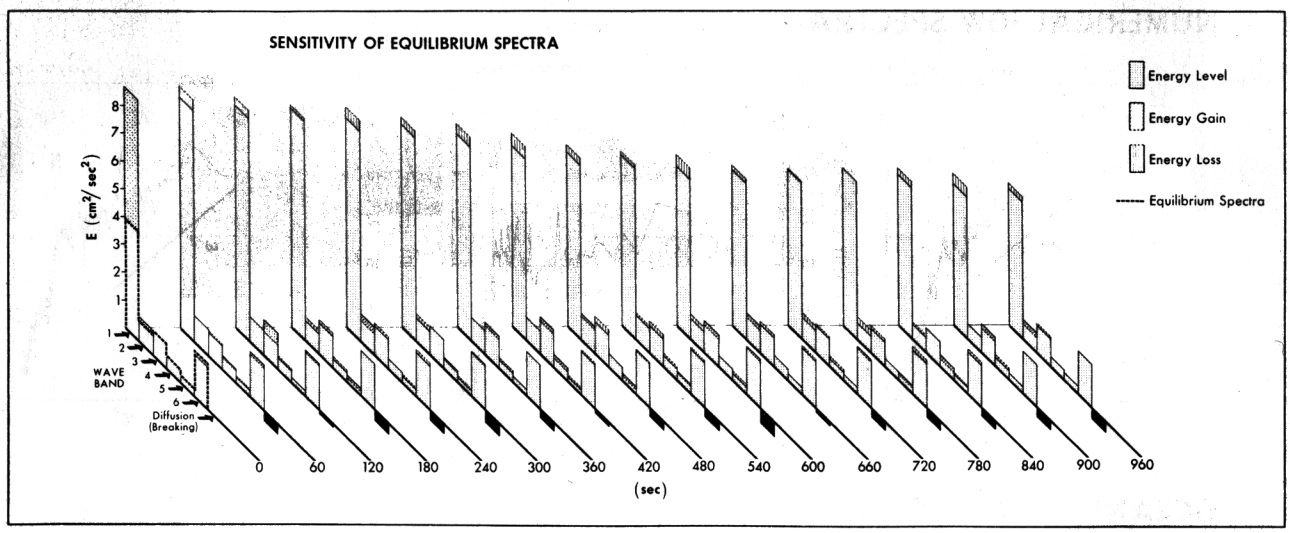

Fig. 16. The same as Figure 10*a* but for the perturbation of the equilibrium state.

cause of the model's strong assumptions, that is, two dimensionality and nonrotation. One may argue that for frequencies far from the inertial frequency, or close to the buoyancy frequency, the rotationless approximation is justified. The justification for two-dimensional is harder to support. It was unclear whether a two-dimensional equilibrium spectrum existed, and if so, what shape it took; this alone justified the study of a two-dimensional simulation. Also, the study of wave-wave interactions requires a large number of waves, and an even larger number if wave breaking is included. At least 50 waves in each direction should be resolved, making any three-dimensional model prohibitively large. The interplay between wave-wave interactions and wave breaking is present in two-dimensional systems. Perhaps this interplay does not have the intensity present in three dimensions, or precisely the same role, but we believe that the physics will be similar and accurately modeled with sufficient resolution. The two-dimensional model will lack interactions found in a three-dimensional simulation; if anything, this should underestimate wave breaking phenomena, as it is well known that three-dimensional systems cascade energy to high wave numbers more readily than two-dimensional systems. With the preceding in mind, we present some recent data on oceanic power spectra [*Eriksen*, 1978] in the lower portion of Figure 18, where the frequency range is well separated from the inertial frequency. Power spectra from the two-dimensional model are shown in the upper portion of Figure 18, and the two sets have some striking similarities. The slopes for frequencies below N are approximately equal, and the rise in the vertical velocity spectra near N is similar. Oceanic spectra fall off less rapidly

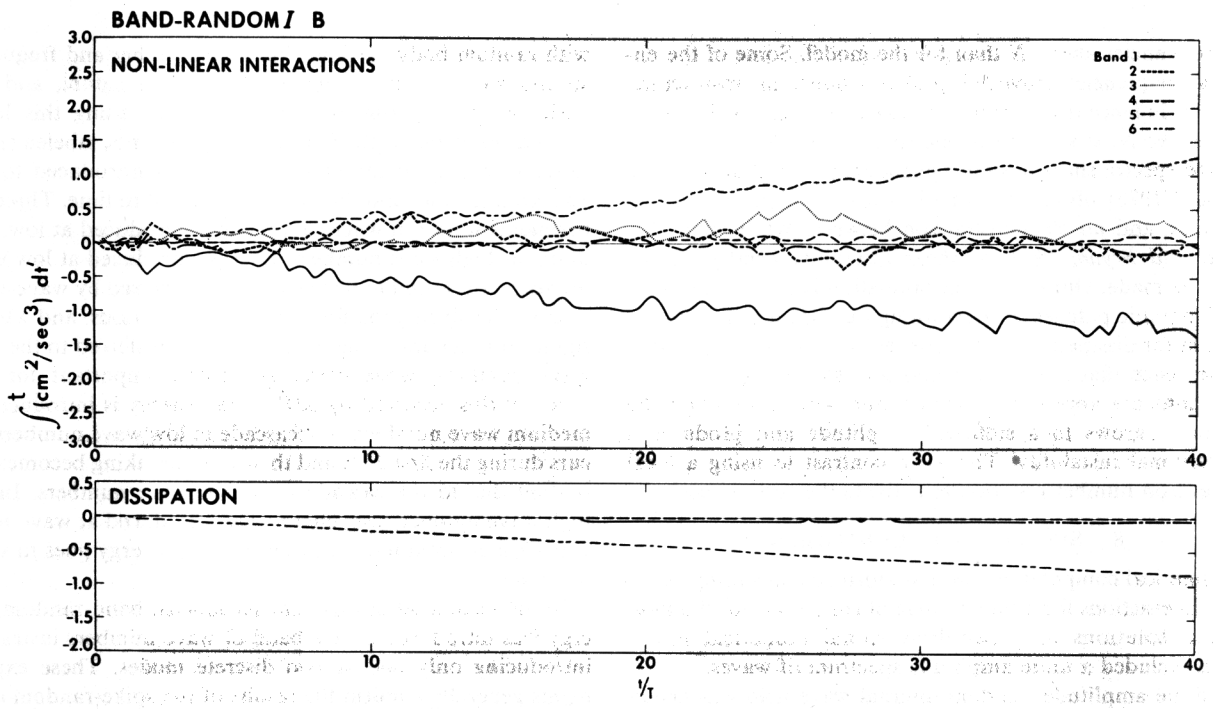

Fig. 17. The same as Figure 13 but for the last experiment.

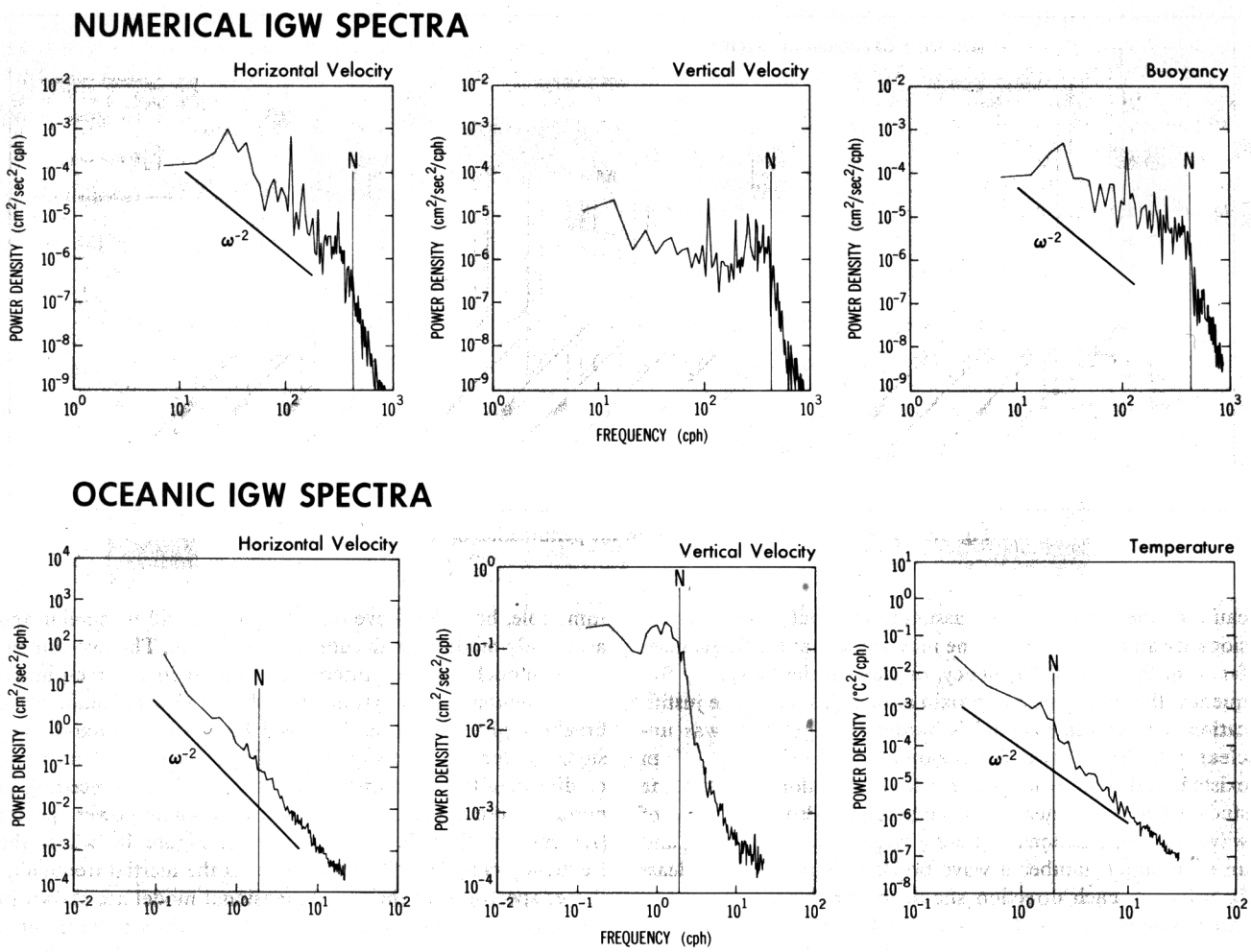

Fig. 18. The upper portion shows spectral densities for horizontal and vertical velocities and buoyancy taken from the numerically generated random internal wave field. The lower portion shows similar spectral densities taken from oceanic observations by *Eriksen* [1978].

for frequencies above N than for the model. Some of the energy at frequencies above N is probably due to microstructure, while turbulence is the prime candidate for the majority of energy above N. If so, the oceanic spectra and the numerically derived spectra share a similar phenomenological description. *Eriksen* [1978] observed sporadic wave breaking at all frequencies, and no clear distinction between overturning [*Orlanski and Bryan,* 1969] or shear instability [*Phillips,* 1966] could be made. Our numerical simulation is one where localized, sporadic patches of overturning (as shown in Figure 11) account for dissipation. The model allows for shear instability in the sence that 'Kelvin-Helmholtz' waves can grow if the conditions are appropriate. Dissipation will occur when the instability grows to a sufficient amplitude and produces a gravitational instability. This is in contrast to using a local Richardson number criterion to activate the eddy viscosity.

8. Summary and Conclusions

Numerical computations were performed concerning wave-wave interactions for a broad range of conditions for the most general solutions of a two-dimensional numerical model which included a finite amplitude spectrum of waves.

A finite amplitude, random internal wave field was generated by a long time integration of the two-dimensional model with random body forcing. The wave number and frequency spectra were relatively smooth and red in nature, and two basic sets of experiments were performed using this background spectrum. In the first set of experiments, labeled spike-random, energy at individual modes was introduced to this background field, and the model integrated in time. Three experiments were run where energy was introduced at low, medium, or high wave numbers. Energy introduced at low wave numbers was found to be effectively transferred by wave-wave interactions during the first 30 buoyancy periods, and when a significant amount of energy had been transferred to the high wave numbers, wave breaking became important for dissipation; this occurred by $60T$. When energy is introduced at medium wave numbers, a decascade to low wave numbers occurs during the first $30T$, and then wave breaking becomes important due to the cascade to higher wave numbers. In the high wave number case, energy was introduced at wave numbers close to saturation, and virtually all energy goes to wave breaking.

In the second set of experiments, labeled band-random, energy was introduced over a band of wave numbers instead of introducing only one or two discrete modes. These experiments generally confirm the results of the spike-random case, and the results were represented in Figures 10*a*–10*c*, where

the time evolution of wave bands is shown along with the dissipative energy loss. The background spectrum appears to be at a saturation level for the high wave numbers but not for the low ones. In the first experiment the energy was introduced at the low wave numbers, and triad interactions accounted for energy transfers during the first 10 buoyancy periods (Figure 13). Subsequently, wave-wave interactions and wave breaking played important roles in the transfer of energy. Wave-wave interactions can represent the excitation of nonresonant forced waves, as well as resonant waves. By the end of this experiment, it seemed that an equilibrium spectrum had evolved. The second experiment introduced energy at medium wave numbers, and both decascading of energy to lower wave numbers and cascading to high wave numbers accounted for the loss of energy from medium wave numbers during the early times. By around $15T$ (180 s), wave breaking became an important feature, as seen in Figure 10*b*, where block 7 grows in amplitude. The system reached an equilibrium from medium wave numbers upward, and the lowest wave numbers did not grow even though they were far from saturated. This point will be taken up later. In the third experiment, energy was introduced at high, although not the highest, wave numbers and energy was rapidly transferred to higher wave numbers where dissipation occurred. Eddy diffusivities for the three band-random experiments were calculated for the gravest mode and found to be of order 1 cm^2 s.

A complementary result to the energy loss or gain by each band in Figures 10*a*–10*c* is described in section 6 (Figures 12*a*–12*c*), where the total energy transfer by nonlinear terms and the viscous dissipation (as parameterized by gravitational overturning) are computed. Those terms are shown as a function of wave number and integrated over time. It was found that the nonlinear advection accounts for smoothing the spectrum over neighboring waves. However, when the equilibrium level was exceeded, the energy flowed directly from low and medium wave numbers to high wave numbers where wave breaking occurred. Dissipation was approximately constant and a function of wave number and a dissipation ratio function was found to be proportional to $k^{5/2}$.

The assumption that the final state reached for band-random experiment I (Figure 10*a*) was an equilibrium spectrum was tested in the last experiment of section 7. An initial input of energy was introduced to the equilibrium spectrum, and the time evolution showed that almost instantly wave breaking dissipated as much or more energy than the redistribution done by wave-wave interaction. This process continues until the level of energy of the low wave number waves is such that no further wave breaking is produced.

The main conclusions of the final set of experiments, along with much of the previous work, can best be described if one assumes a sequence of steps whereby the energy level is gradually increased. Multiple triad interactions will result in a filling of the energy spectrum when energy is introduced in a particular band of wave numbers. For bands where the energy level is high enough to result in nonlinear time scales of only a few intrinsic periods, wave-wave interactions (resonant and nonresonant) provide the mechanism for filling the spectrum. The energy transfer becomes more and more rapid with increasing energy, and no universal spectrum appears to result from these processes. As the energy input increases, energy will accumulate in high wave numbers until localized instabilities (overturning) occurs. From that point on, these high wave numbers will remain at a saturation level such that any additional energy input at the saturated band, either directly or via wave-wave interactions, will result in localized mixing. On the other hand, additional energy input at bands other than the saturated band will result in an increase of low and medium wave band energy (via wave-wave interactions) until an equilibrium level is achieved. The equilibrium level of any particular band will depend on the high wave number bands being saturated. For instance, any energy above the equilibrium at low wave numbers will produce localized mixing in physical space almost instantaneously. This does not mean that the low wave numbers are saturated, as their energy levels can be much lower than a saturation level. What takes place at or near an equilibrium level is that the contributions from high and low wave numbers result in localized regions in the physical space where the criterion for instability is almost met. In fact, this superposition effect means that low and medium wave numbers are far from meeting any breaking criterion when taken individually, yet cannot tolerate any additional input energy when in the presence of a saturated band of high wave numbers.

It is clear that the sporadic, localized patches of turbulence in physical space are by no means localized in wave number space. Even though a band of saturated high wave numbers is necessary to produce the localized mixing, a continuous cascade through all the scales from low to high wave numbers is not necessary. Consider the case of overturning, where the criterion is that the total vertical density gradient must reverse sign at some point in space. Suppose that a low and a high wave number are superimposed such that the criterion for gravitational instability is nearly met. Energy input at the low wave number will produce a region in space where this criterion is met and results in overturning without a continuous energy cascade from low to high wave number. This statement must be qualified, as overturning is a manifestation of gravitational instability. The long waves are stable to infinitesimal perturbations and cannot be considered in saturation, but the superposition with small but finite short waves makes the system unstable to finite amplitude perturbations, as a consequence producing short waves that are efficiently dissipated.

Once an equilibrium amplitude is reached, wave-wave interactions are inefficient for transferring energy from band to band. On the other hand, energy is very rapidly dissipated by overturning when energy is introduced. Well-defined criteria for overturning or mixing are possible in physical space, but no simple criteria can be given involving wave number space because of the complex superposition of many waves. Certainly more sophisticated numerical experiments using either finite difference or spectral methods which include important effects such as rotation, three dimensionality, and stratification variability will give a more quantitative estimation of energy budgets for internal gravity waves in the ocean. But the qualitative picture given by this simple model may still prove to be accurate. Ocean experiments can test some of the suggested hypotheses by measuring the intensity of dissipation as a function the distance from an energy source (oceanic ridge, etc.). The present results predict that the dissipation will be proportional to the deviation of the spectral energy level from that of the 'universal' spectrum.

Acknowledgments. The authors wish to thank P. Ripa and G. Philander for their comments and L. Polinsky for programing and analysis work. We also thank J. Kennedy and B. Williams for typing the

manuscript, and P. Tunison for scientific illustrations. One of the authors (C.P.C.) was supported by a NOAA grant 04-7-022-44017, and the experimental laboratory facilities were supported by National Science Foundation grant ATM77-19955.

REFERENCES

Bretherton, F. P., Resonant interaction between waves, The case of discrete oscillations, *J. Fluid Mech., 20,* 457–479, 1964.

Cairns, J. L., Internal wave measurements from a midwater float, *J. Geophys. Res., 80,* 299–306, 1975.

Charnock, H., A preliminary study of the directional spectrum of short period internal waves, Proceedings of the 2nd U.S. Navy Symposium on Military Oceanography, pp. 175–178, 1965.

Davis, R. E., and A. Acrivos, Solitary internal waves in deep water, *J. Fluid Mech., 29,* 593–608, 1967.

Eriksen, C. C., Measurements and models of fine-structure, internal gravity waves, and waves breaking in the deep ocean, *J. Geophys. Res., 83,* 2989–3009, 1978.

Fofonoff, N. P., and F. Webster, Current measurements in the Western Atlantic, *Phil. Trans. R. Soc., Ser. A, 270,* 423–436, 1971.

Frankignoul, C. J., Stability of finite amplitude internal waves in a shear flow, *Geophys. Fluid Dynamics, 2,* 225–264, 1972.

Garrett, C. J. R., and W. H. Munk, Space-time scales of internal waves, *Geophys. Fluid Dynamics, 2,* 225–264, 1972*a*.

Garrett, C. J. R., and W. H. Munk, Oceanic mixing by breaking internal waves, *Deep Sea Res., 19,* 823–832, 1972*b*.

Garrett, C. J. R., and W. H. Munk, Space-time scales of internal waves: A progress report, *J. Geophys. Res., 80,* 291–297, 1975.

Gould, W. J., W. J. Schmitz, and C. Wunsch, Preliminary field results for a mid-ocean dynamics experiment (MODE-0), *Deep Sea Res., 21,* 911–932, 1974.

Hasselmann, K., Feymann diagrams and interaction rules of wave-wave scattering processes, *Rev. Geophys., 4,* 1–32, 1966.

Hasselmann, K., Nonlinear interactions treated by the methods of theoretical physics (with application to the generation of waves by wind), *Proc. R. Soc. London, Ser. A, 299,* 77–100, 1967.

Hayes, S. P., Preliminary measurements of the time-lagged coherence of vertical temperature profiles, *J. Geophys. Res., 80,* 307–311, 1975.

Katz, E. J., Tow spectra from Mode, *J. Geophys. Res., 80,* 1163–1167, 1975.

LaFond, E. C., The use of bathythermographs to determine ocean currents, *Eos Trans. AGU, 30,* 231–237, 1949.

Leaman, K. D., and T. B. Sanford, Vertical energy propagation of inertial waves: a vector spectral analysis of velocity profiles, *J. Geophys. Res., 80,* 1975–1978, 1975.

Martin, S., W. F. Simmons, and C. Wunsch, The excitation of resonant triads by single internal waves, *J. Fluid Mech., 53,* 17–44, 1972.

McComas, C. H. and F. P. Bretherton, Resonant interactions of oceanic internal waves, *J. Geophys. Res., 82,* 1397–1412, 1977.

McEwan, A. D., D. W. Mander, and R. K. Smith, Forced resonant second-order interactions between damped internal waves, *J. Fluid Mech., 55,* 589–608, 1972.

Müller, P., and D. J. Olbers, On the dynamics of internal waves in the deep ocean, *J. Geophys. Res., 80,* 3848–3859, 1975.

Müller, P., D. J. Olbers, and S. Willebrand, The IWEX spectrum, *J. Geophys. Res., 83,* 479–500, 1978.

Orlanski, I., On the breaking of standing internal gravity waves, *J. Fluid Mech., 54,* 577–598, 1972.

Orlanski, I., and K. Bryan, Formation of the thermocline step structure by large amplitude internal gravity waves, *J. Geophys. Res., 74,* 6975–6983, 1969.

Orlanski, I., and C. P. Cerasoli, Resonant and non-resonant wave-wave interactions for internal gravity waves, in *Marine Turbulence, Oceanogr. Ser.,* Elsevier, New York, 1979.

Orlanski, I., and B. B. Ross, Numerical simulation of generation and breaking of internal gravity waves, *J. Geophys. Res., 78,* 8806–8826, 1973.

Orlanski, I., B. B. Ross, and L. J. Polinsky, Diurnal variation of the planetary boundary layer in a mesoscale model, *J. Atmos. Sci., 31,* 965–989, 1974.

Phillips, O. M., *The Dynamics of the Upper Ocean.* Cambridge University Press, New York, 1966.

Phillips, O. M., *The Dynamics of the Upper Ocean,* 2nd ed., Cambridge University Press, New York, 1977.

Thorpe, S. A., The excitation, dissipation, and interaction of internal waves in the deep ocean, *J. Geophys. Res., 80,* 328–338, 1975.

Webster, F., Vertical profiles of horizontal ocean currents, *Deep Sea Res., 16,* 85–98, 1969.

(Received January 30, 1980;
revised May 27, 1980;
accepted September 30, 1980.)